

CZECH TECHNICAL UNIVERSITY IN PRAGUE  
FACULTY OF ELECTRICAL ENGINEERING  
DEPARTMENT OF CYBERNETICS



## MASTER'S THESIS

3D map estimation from a single RGB image

**Author:** Bc. Matěj Račinský

**Thesis supervisor:** doc. Ing. Karel Zimmermann, PhD.

**Thesis co-supervisor:** Ing. Tomáš Petříček

In Prague, May 2018



## I. OSOBNÍ A STUDIJNÍ ÚDAJE

Příjmení: **Račinský** Jméno: **Matěj** Osobní číslo: **420368**  
Fakulta/ústav: **Fakulta elektrotechnická**  
Zadávající katedra/ústav: **Katedra počítačů**  
Studijní program: **Otevřená informatika**  
Studijní obor: **Umělá inteligence**

## II. ÚDAJE K DIPLOMOVÉ PRÁCI

Název diplomové práce:

**Odhad 3D mapy z jednoho RGB obrazu**

Název diplomové práce anglicky:

**3D map estimation from a single RGB image**

Pokyny pro vypracování:

Development of reliable algorithms for self-driving cars has recently attracted substantial attention of researchers and industry. Accurate 3D local map estimation is an essential component for many fundamental capabilities such as emergency braking or safe turning on a road intersection. Consequently, any fully-autonomous vehicle requires an algorithm which process low-level data such as RGB or RGBD measurements and provides a medium-level interpretation such as 3D local voxel map with semantic object categories. 1. Familiarize yourself with publicly available GTA5 interface, which has been recently shown to be realistic enough to improve state-of-the-art object detectors [1].  
2. Study state-of-the-art methods for object detection, semantic segmentation and 3D mapping such as [2,3,4].  
3. Propose deep convolutional neural network suitable for local 3D voxel map estimation from RGB images. Focus mainly on a simple case of independent reconstruction from a single RGB image.  
4. Train and evaluate the proposed network on data generated by GTA5 interface [1]. Discuss typical failure cases.  
5. Optionally propose, train and evaluate method for segmentation of voxels belonging to dynamic object such as moving cars or pedestrian

Seznam doporučené literatury:

[1] Driving in the Matrix, ICRA, 2017, <https://arxiv.org/pdf/1610.01983.pdf>, <https://github.com/umautobots/driving-in-the-matrix>  
[2] K.He, G. Gkioxari, P. Dollar, R.Girshick, Mask R-CNN, ICCV 2017, <https://arxiv.org/abs/1703.06870>, [https://github.com/matterport/Mask\\_RCNN](https://github.com/matterport/Mask_RCNN)  
[3] X. Han, Z. Li, H. Huang, E. Kalogerakism and Y. Yu. High-Resolution Shape Completion Using Deep Neural Networks for Global Structure and Local Geometry Inference. ICCV 2017 <https://arxiv.org/abs/1709.07599>  
[4] C. B. Choy, D. Xu, J. Gwak, K. Chen, and S. Savarese. 3DR2N2: A unified approach for single and multi-view 3D object reconstruction. ECCV 2016 <https://arxiv.org/abs/1604.00449>

Jméno a pracoviště vedoucí(ho) diplomové práce:

**doc. Ing. Karel Zimmermann, Ph.D., vidění pro roboty a autonomní systémy FEL**

Jméno a pracoviště druhé(ho) vedoucí(ho) nebo konzultanta(ky) diplomové práce:

Datum zadání diplomové práce: **08.02.2018**

Termín odevzdání diplomové práce: **25.05.2018**

Platnost zadání diplomové práce: **30.09.2019**

doc. Ing. Karel Zimmermann, Ph.D.  
podpis vedoucí(ho) práce

podpis vedoucí(ho) ústavu/katedry

prof. Ing. Pavel Ripka, CSc.  
podpis děkana(ky)

### III. PŘEVZETÍ ZADÁNÍ

Diplomant bere na vědomí, že je povinen vypracovat diplomovou práci samostatně, bez cizí pomoci, s výjimkou poskytnutých konzultací. Seznam použité literatury, jiných pramenů a jmen konzultantů je třeba uvést v diplomové práci.

\_\_\_\_\_  
Datum převzetí zadání

\_\_\_\_\_  
Podpis studenta

**Author statement for the graduate thesis:**

I declare that the presented work was developed independently and that I have listed all the sources of information used within it in accordance with the methodical instructions for observing the ethical principles in the presentation of university theses.

Prague, date \_\_\_\_\_

\_\_\_\_\_  
signature



**Název práce:** Odhad 3D mapy z jednoho RGB obrazu

**Autor:** Bc. Matěj Račinský

**Katedra (ústav):** Katedra počítačů

**Abstrakt** Tato práce se zabývá využitím virtuálních světů z počítačových her jakožto zdroje dat pro strojové učení, a odhadem voxelové mapy z jednoho RGB obrázku za pomoci hlubokého učení. Tato práce zahrnuje skripty pro napojení se na PC hru GTA V a sběr dat z ní pro tvorbu automaticky anotovaných datasetů, a implementaci hluboké neuronové sítě v TensorFlow.

**Klíčová slova:** Hluboké učení, Strojové učení, GTA V, virtuální svět, odhad hloubky, odhad voxelové mapy, RAGE

---

**Title:** 3D map estimation from a single RGB image

**Author:** Bc. Matěj Račinský

**Department:** Department of Computer Science

**Abstract** In this thesis we explore virtual worlds used as data source for machine learning and voxel map estimation from single RGB image with deep learning. This thesis describes principles and implementation of hooking into GTA V and gathering data from it to create automatically annotated dataset, and implementation of deep neural network in TensorFlow.

**Keywords:** Deep learning, Machine learning, GTA V, virtual world, depth estimation, voxel map estimation, RAGE

# CONTENTS

<b>1. Introduction</b>	<b>10</b>
1.1. Obtaining large annotated datasets for high-capacity models . . . . .	10
1.1.1. Manual annotation services . . . . .	11
1.1.2. Generating synthetic datasets from game engines . . . . .	11
1.2. Thesis Contribution . . . . .	12
1.2.1. Thesis structure . . . . .	12
<b>2. Related work</b>	<b>13</b>
2.1. Using Computer Games for Machine Learning . . . . .	13
2.2. 3D map estimation . . . . .	13
2.2.1. Deep convolutional neural networks . . . . .	14
2.2.2. Residual networks . . . . .	15
2.2.3. Depth estimation . . . . .	16
2.2.4. 3D map estimation . . . . .	17
<b>3. Transforming GTA V into the State of the Art simulator</b>	<b>18</b>
3.1. GTA V introduction . . . . .	18
3.1.1. Cars . . . . .	19
3.1.2. Pedestrians . . . . .	19
3.2. Automotive Simulators . . . . .	19
3.3. GTA V modding ecosystem . . . . .	19
3.4. Simulation environment and development stack . . . . .	20
3.5. GTA V native API and data obtaining . . . . .	22
3.5.1. Image data . . . . .	22
3.5.2. Rendering pipeline data . . . . .	23
3.5.3. GTA V internal data . . . . .	25
3.6. Reverse-engineering the RAGE rendering pipeline . . . . .	30
3.6.1. Object to World Coordinates . . . . .	31
3.6.2. World to Camera Coordinates . . . . .	31
3.6.3. Camera to NDC . . . . .	32
3.6.4. NDC to Window Coordinates . . . . .	33
3.7. VirtualScapes Dataset proposal . . . . .	34
<b>4. 3D map estimation</b>	<b>38</b>
4.1. TensorFlow . . . . .	38
4.2. Depth estimation . . . . .	38
4.3. 3D map estimation . . . . .	41
4.3.1. Training dataset construction from depth images . . . . .	41
4.3.2. Metrics and network setup . . . . .	44



<b>5. Experiments</b>	<b>49</b>
5.1. Reverse engineering the true Far Clip . . . . .	49
5.2. Depth estimation . . . . .	54
5.3. 3D map estimation . . . . .	59
<b>6. Conclusion and Future Work</b>	<b>62</b>
<b>Bibliography</b>	<b>63</b>
<b>A. Contents of the enclosed CD</b>	<b>69</b>

## INTRODUCTION

The main aim of this thesis is reactive 3D map estimation from single RGB image. The task of building 3D map is essential procedure in many robotics tasks and is then utilized in high-level planning. For many static environments, like buildings and roads, we have detailed maps available which are being used for this task. But for other environments, with lots of cars like in parking lots or crossroads, or off-road trajectories, the pre-calculated 3D map is not available and it needs to be created online. There are multiple approaches for 3D map estimation, lots of them using depth measurements. Often used approach is utilization of depth measurements and then building 3D map which is continuously updated during movement. This is a complicated task due to matching newly obtained data on existing 3D map. This thesis describes an approach based on reactive mapping without the need to build long-term internal world representation, using only immediate sensor input. Only RGB camera input is used for 3D map reconstruction instead of depth measurements. The RGB image has many advantages, RGB cameras are cheap and in higher resolution than depth sensors. RGB camera is a passive sensor, so multiple RGB cameras won't interfere with each other unlike LiDARs, so the RGB image can be obtained easily. Due to the problem of obtaining dense and precise ground truth, this thesis exploits usage of synthetic datasets as a fast and efficient way to obtain ground truth for such task. GTA V is used here as a simulator for the creation of a synthetic dataset.

### **1.1. Obtaining large annotated datasets for high-capacity models**

In recent years, both machine learning and deep learning has experienced great progress in many fields [60]. Deep learning has outperformed many other machine learning approaches by using deep, high-capacity models trained on large datasets. Especially in the field of computer vision, neural networks achieve state of the art results in most of the tasks. Many tasks in computer vision are the first where deep neural networks achieve state of the art results before being used in other fields, and in this field, deeper and deeper architectures are being proposed earlier than in other fields. With larger amount of parameters, the need for large datasets is growing, with current datasets unable to cover the need for annotated data.

Data has proven to be limiting factor in many computer vision tasks. The main problem is that manual data annotation is exhausting, time-consuming and costly. That is even more significant for pixel-wise annotation which is crucial for tasks of semantic segmentation. Pixel-

wise annotated datasets are orders of magnitude smaller than image classification datasets. This is sometimes called “curse of dataset annotation” [58], because more detailed semantic labelling leads to smaller size of dataset.

Many novel neural network architectures are being proposed every year because of ongoing research and increasing computing power. With growing capacity and number of parameters in these new models, there is need for bigger and bigger datasets for training. Several papers shown positive correlation between the size of data and performance [29, 49, 53].

### 1.1.1. Manual annotation services

There are attempts to develop tooling necessary to speed up the manual annotation process during datasets creation, most known being the Amazon Mechanical Turk (AMT) [19] and Supervise.ly [6].

Amazon Mechanical Turk is a platform for crowdsourcing work and has been used in many academic fields. AMT is a “marketplace for work that requires human intelligence” [1], a web-based platform for distributing tasks to a pool of human workers, known colloquially as Turkers. These tasks are typically small (i.e. a few minutes to perform a task rather than days or weeks) and payments pay task are low, in the orders of cents per task. This platform provides possibility to distribute the annotation process among many people at once and for low price. Although still being manual, it accelerates the annotation process and helps researchers to annotate data more easily [51]. Quality of work can not be guaranteed since task provider can’t supervise workers and correct them manually, but this disadvantage can be compensated by various quality assurance approaches [51]. Supervise.ly is another web-based platform, focused on computer vision datasets annotation. It provides helpful tooling for annotators in unified web interface, speeding up the annotation process. It offers integration with the AMT, so together, they seem to be candidate for industrial standard of data annotation.

Although these tools lead to faster annotation process at lower cost, it still can not be compared to the fully automated data gathering and annotation, which could potentially solve these problems of lack of datasets in many computer vision and related tasks. The power of automatic annotation can be also expressed in terms of money. Although not many manually annotated datasets describe time of annotation, some of them do. In Cityscapes, the fine annotation took 1.5 hour per image [17]. If we had annotators paid minimum hourly wage in USA, 7.25\$, what would mean each fine annotated image has price 10.875\$. The whole fine annotated Cityscapes dataset with 5000 images thus have has price at least 54 375\$ and took 312.5 days to annotate. In the dataset I created as part of my thesis, I gathered 33292 images in 3.5 hours. If we would annotate this dataset same as Cityscapes fine annotation, it would take over 2080 days, which is approximately 5.7 years, and it would cost 362 050\$. Now we can see how this automatic annotation approach is significantly both time and money saving.

### 1.1.2. Generating synthetic datasets from game engines

In last decades, gaming industry has grown hugely and expanded from small and specific community into public society and became mainstream industry. The gaming industry became big driving force in many fields, and indirectly influenced even machine learning. The mainstream model of gaming is on personal computers, where each player has his own gaming PC, along with console gaming. Thanks to ever-growing number of players, lots of money got into industry and the growing demand for better graphics in games led to big improvements in both software-

computer graphics and hardware-graphics cards. With lots of money being invested by players in their PCs, GPU manufacturers were able to deliver more powerful GPUs every year and we can see exponential growth of GPU computational power [55].

Big companies in gaming industry have enough resources to develop the state of the art real-time computer graphics, which can we see in their products, AAA games with graphics very near to reality. Recent papers [35, 45] have shown that we can use screenshots from PC games to obtain large automatically or semi-automatically annotated datasets, which improve learning. This lets us to outperform same models trained only on real data and achieve state of the art results on public datasets (KITTI dataset in [35] and CamVid dataset in [45]).

Other approaches utilizing computer games for machine learning have appeared recently, one of the most known being OpenAI Gym, software platform providing reinforcement learning framework [13]. Later, Universe [43] has been released, designed to turn various computer games into OpenAI Gym environment, easing to deploy same reinforcement learning algorithms into many different virtual worlds, but due to legal issues, they require permission from the game owner to integrate particular game into the Universe.

## **1.2. Thesis Contribution**

In this thesis, I propose deep convolutional neural network for 3D map estimation. For this task, I leverage synthetic data from rich virtual worlds in form of synthetic dataset and propose software architecture for dataset creation. Then I create data for training in form of pairs of RGB image capturing space in front of car, and voxelmap of that space. In the last part, Then I empirically evaluate multiple setups of predictions of both depth estimation and 3D map estimation

### **1.2.1. Thesis structure**

This thesis is structured as follows. Chapter 2 covers related work and previous achievements of synthetic datasets. Chapter 3 describes game Grand Theft Auto V and its utilization in creating synthetic datasets, this part serves as a documentation for using libraries for manipulating the GTA world. Here I describe whole modding process, the game API, internal game coordinate systems and data which can be obtained from the game. Chapter 4 describes voxel map estimation from a single RGB image with network architecture and data preparation. It is followed by chapter 5, where I describe all experiments done as part of this thesis. Last chapter contains conclusion of the whole thesis.

## RELATED WORK

### 2.1. Using Computer Games for Machine Learning

Richter et al. [45] used GTA V to obtain screenshots and performed semi-automated pixel-wise semantic segmentation. Although the process was not fully automatic, the annotation speed per image was drastically increased, being 771 times faster than fine per-image annotation of Cityscapes [17] and 514 times faster than per-image annotation of CamVid [14]. Richter et al. extracted 24 966 images from game GTA V, which is roughly two orders of magnitude larger than CamVid and three orders of magnitude larger than semantic annotations for KITTI dataset. They trained the prediction module of Yu and Kolthun [59] and by using on  $\frac{1}{3}$  of the CamVid training set (which is ) and all 24 966 GTA V screenshots, they outperformed same model trained on whole CamVid training dataset.

For images extraction, they use RenderDoc[36], stand-alone graphics debugger. It intercepts the communication between the game and the GPU and allows to gather screenshots. It's advantage is that it can be used for different games, allowing to gather datasets in various environments.

Johnson-Roberson et al. [35] used GTA V screenshots, depth and stencil buffer to produce car images and automatically calculated their bounding boxes.

On these generated data, they trained Faster R-CNN [44] only on screenshots from the GTA V game, using up to 200 000 screenshots, which is one order of magnitude bigger than Cityscapes dataset. Using only screenshots for training, they outperformed same architecture trained on Cityscapes, evaluating on KITTI dataset. They developed their own GTA V mod3.3 to hook into GPU calls and gather screenshots from here.

GTA V has also been used as a part of the OpenAI Universe, promising powerful environment for machine learning, but due to Rockstar Games Terms of Services, it has been removed and is not currently supported by the OpenAI Universe. Nowadays, OpenAI Universe supports many games, but focuses mainly on Reinforcement Learning, and thus allows only communication with games through a strict API and does not allow the complex setup and modifications of the game described in this thesis.

### 2.2. 3D map estimation

3D map estimation is a complex an important task in computer vision, and many approaches have been used in attempts to solve this task. It is tightly coupled to the depth estimation, because

the most important part of the 3D estimation is to estimate the depth of objects on the image, since spatial information about horizontal and vertical position is contained in the image directly. Most studies focus on binocular cameras [48], also called stereo vision where depth and 3D map is reconstructed using information from two cameras, and thus depth and position in 3D can be estimated from seeing same points from different views. The other approach is to use only single image, without the binocular information. That task is more challenging due to lack of information from the second image, and even the State of the Art approaches fall short compared to the binocular vision. But thanks to the recent success of deep convolutional neural networks, there have been advances in monocular depth estimation.

### 2.2.1. Deep convolutional neural networks

In machine learning, deep convolutional neural networks have been used more and more mostly due to significant breakthroughs in image classification tasks. Advantage of deep neural networks is the capability to naturally utilize low-level, mid-level, and high-level features, without need for manual feature-engineering and lets us train whole architectures end-to-end. Recent results [50, 54] in visual recognition tasks, mostly on ImageNet dataset [46], reveal depth of network plays crucial role in model accuracy and started the revolution in many computer vision tasks [39].

Neural networks are machine learning models vaguely inspired by the biological neural networks that constitute human brains. Neural networks are being used as universal approximators, theoretically capable of arbitrarily accurate approximation to an arbitrary function [33] and thus are used for many different tasks, for instance classification, regression, clustering, and many other. The neural network, as name suggests, is network of interconnected artificial neurons. An artificial neuron is based on biological neuron, but with many simplifications. It consists of inputs to the neuron (inspired by dendrites), the neuron itself, and the output of the neuron (inspired by axon). Intuitively the artificial neuron sums all inputs weighted by neuron weights and send them to into its activation function, inspired by axon. Formally, the output of neuron  $y$  with inputs  $\mathbf{x} = (x_0, \dots, x_n)$ , weights  $\mathbf{w} = (w_0, \dots, w_n)$ , bias  $\beta$  and activation function  $\varphi(\cdot)$  is defined as

$$y = \varphi \left( \beta + \sum_{i=0}^n w_i x_i \right) = \varphi (\mathbf{w} \cdot \mathbf{x} + \beta)$$

. In its typical architecture, the neural network comprises of many layers stacked on top of each other, with output of neurons in one layer connected to all inputs of all neurons in the next layer and information flows from each neuron of previous layer to each neuron of next layer. This is called fully-connected neural network. Other approach is to connect inputs of a neuron only to a subset of neurons in previous layers, specifically its corresponding neuron in previous layer and its neighbours. This dramatically reduces number of parameters needed to be learned. The neural network is then usually learned end-to-end by the back-propagation algorithm [37] which minimizes the loss function using stochastic gradient descent or its alternatives.

When neural network has many layers stacked on top of each other, it is called a deep neural network. The success of deep neural networks lies in their abilities to approximate non-trivial function because of high number of parameters of the network. The disadvantage of deep neural networks is the time they need to learn because it takes days or weeks to train state of the art deep neural networks.

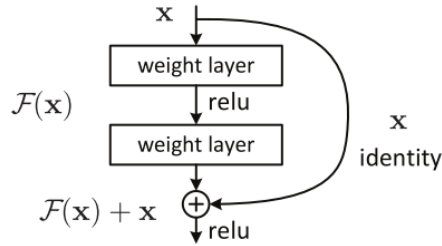


Figure 2.1.: Residual and shortcut layers[30]

## 2.2.2. Residual networks

As mentioned above, deep network became very popular and widely used in computer vision and machine learning. But there are some caveats when building a new deep architecture for neural network. When deeper networks were created simply by stacking more and more layers in the model, these models become hard to train. One of these problems is the notorious vanishing gradient, which is being addressed by many approaches, like normalized initialization [27, 38] and normalization layers [34]. Other problem is the degradation problem, where training accuracy starts to worsen, after stacking more layers [52]. Residual networks aim to address this problem of degradation.

If shallower model is able to learn with higher accuracy than deeper model, we want the deeper model to be able to learn at least same as shallower one, or better. If we stack a new layer into the model, we want them to be able to learn identity mapping. Then the model with new layers will behave same as shallower model during prediction. Experiments show that current solvers using gradient descent are not able to find such solution which would let newer layer to learn identity mapping in feasible time. The residual learning aims to tackle this problem by explicitly learning the residual mapping instead of original mapping. If we want our newly stacked layers to represent mapping  $\mathcal{H}(\mathbf{x})$ , instead we let them learn another mapping  $\mathcal{F}(\mathbf{x}) = \mathcal{H}(\mathbf{x}) - \mathbf{x}$ . The original mapping we aim to,  $\mathcal{H}(\mathbf{x})$  is then reconstructed as  $\mathcal{H}(\mathbf{x}) = \mathcal{F}(\mathbf{x}) + \mathbf{x}$ . He et al. [30] shows it is easier to learn the residual mapping than to learn the original mapping. It also more easily preserves the identity mapping, if  $\mathcal{F}(\mathbf{x}) = \mathbf{0}$ , because it is easier to fit these layers to zero than to explicitly learn identity mapping.

The formulation of  $\mathcal{F}(\mathbf{x}) + \mathbf{x}$  can be realized by feed-forward neural network with shortcut connections [9], also known as skip connections. The advantage of this approach is it can be easily implemented in current neural network frameworks out of the box, and it whole network can still be learned by SGD end-to-end without any further modifications. Intuitively, the identity mapping, shortcut connection can be seen as an information highway, where information flows unchanged both forwards and backwards without any changes. He et al. [30] show the residual learning lets us train very deep models and present several architectures based on residual learning: ResNet-18, ResNet-34, Resnet-50, ResNet-101, and ResNet-152. basically ResNet architecture consists of 4 residual blocks, repeated many times. The difference between individual architectures is only in number of repetitions these residual blocks.

Residual networks have been widely adopted as a part of many upcoming architectures for various tasks. They are utilized in many image mapping tasks, for instance depth prediction or semantic segmentation. He et al. [31] used ResNet as a backbone for their Mask R-CNN architecture for pixel-wise semantic segmentation and trained on COCO dataset. Their setup



Figure 2.2.: Synthetic image labelled by Mask R-CNN

works well on both real photos and synthetic images, as can be seen in figure 2.2 where image from synthetic dataset is being labelled.

### 2.2.3. Depth estimation

Depth estimation is one of the most fundamental tasks in computer vision. Most existing methods [21, 40] formulate depth estimation as a regression task due to the continuous nature of depth values. Those models for depth estimation are usually trained to minimize L2 norm between ground truth and predicted depths. However it shows that regressing to exact depth is difficult task. In many applications, depth can be known only approximately. With aforementioned approach, I approximate the regression formulation of depth estimation with classification problem. Thus instead of training to predict exact depth, we predict only depth range, still small enough to be useful for our application. Advantage of classification formulation of the problem is that after applying softmax on output of neural network, depths are naturally predicted as confidence in form of probability that particular depth level is occupied [15]. Most notable methods [15, 41] use deep convolutional networks based on famous object classification architectures.

Li et al. [41] use architecture based on deep residual network [30], specifically Resnet-152. The architecture is modified, it does not use the fully connected layer in the end of the network, which drastically decreases the number of trainable parameters, and instead it appends one convolutional and one deconvolutional layer. Also, Li et al. utilize the hierarchical fusion, where output of each block of ResNet is concatenated to other outputs, with dropout layer afterwards, then the network utilizes both low-level and high-level features of the input image during the final layers of depth estimation. The output of final layer is 120x160x200, meaning it outputs 120x160 pixels image with 200 depth levels. The depth space is equally discretized in log space. Specifically,

$$l = \text{round} \left( \frac{\log(d) - \log(d_{min})}{q} \right)$$

where  $l$  is the quantized label,  $q$  is the width of quantization bin,  $d$  is the continuous depth value and  $d_{min}$  is the minimum depth value in the dataset.

Other notable approach of Li et al. is soft weighted sum inference. Usually, the depth is



reconstructed intuitively as a centre of depth bin with maximum value pixel-wise [15]. The last layer is softmax, so values can be interpreted as probabilities of each depth bin being being correct one. Thus the output contains probability distribution of depth pixel-wise. Li et al. [41] reconstruct depth as a soft weighted sum inference by

$$\hat{d} = \exp \{ \mathbf{w}^T \mathbf{p} \}, w_i = \log(d_{min}) + q \cdot i$$

where  $\mathbf{w}$  is the weight vector of depth bins,  $i$  is bin index,  $\mathbf{p}$  is the output score, and  $\hat{d}$  is reconstructed depth.

Then the model is trained end-to-end to minimize the pixel-wise multinomial logistic loss

$$L = - \left[ \sum_{i=1}^N \sum_{k=1}^K 1 \{ D_k = D_i^* \} \log \left( p_i^{D_k} \right) \right] \quad (2.1)$$

where  $N$  is the number of pixels,  $K$  is the number of depth bins,  $D_i^*$  is ground truth depth on pixel  $i$ , and  $p_i^{D_k}$  is the probability of pixel  $i$  to be labelled with  $D_k$  depth bin.

The classical multi-class classification assumes categorical labels without any ordering defined. However depth bins are ordinal labels, not categorical, because they have defined ordering and semantically it makes sense to take into account distance between correct and predicted label during training. This approach is not usable for categorical data, but for nominal data, this knowledge can be used to provide more information for the learning. Cao et al. [15] propose modified loss function which takes distance between depth bins into account. They use similar architecture, with pixel-wise multinomial logistic loss, but with slight modification. In usual logistic loss, the loss is non-zero only for correct label, due to the  $1 \{ D_k = D_i^* \}$  part of the function. Cao et al. propose ‘‘information gain’’ [15] instead, where  $1 \{ D_k = D_i^* \}$  is replaced by  $H(D_i^*, D_k)$ , where  $H$  is  $B \times B$  symmetric matrix with elements  $H(p, q) = \exp(-\alpha(p - q)^2)$  where  $\alpha$  is a constant. This information gain matrix lets the SGD propagate the error not only through correct label and preceding softmax layer, but also through its neighbouring labels, which helps updating the network parameters. So the modified loss is

$$L = - \left[ \sum_{i=1}^N \sum_{k=1}^K H(D_i^*, D_k) \log \left( p_i^{D_k} \right) \right] \quad (2.2)$$

#### 2.2.4. 3D map estimation

Choy et al. [16] use an LSTM framework extended for 3D representation reconstruction, called 3D Recurrent Neural Network for reconstructing 3D images from single or multiple images and perform State of the Art results on single-view reconstruction. In their setup they used encoder-decoder architecture with  $127 \times 127$  input images and  $32 \times 32 \times 32$  voxelmap and trained it to minimize the softmax cross-entropy loss. This setup too learns on synthetic data, using mostly CAD models. This approach is heavily focused on one object dominating the input image which is suited for precise 3D map estimation, but not much for estimation of 3D map of whole scene, usually with multiple objects.

## TRANSFORMING GTA V INTO THE STATE OF THE ART SIMULATOR

In this thesis, Grand Theft Auto V (GTA V) game is used for creating synthetic, nearly photo-realistic dataset.

### 3.1. GTA V introduction

GTA V is action-adventure open-world video game developed by Rockstar North and published by Rockstar Games. The game was released on 17.9.2013 for PlayStation 3 and Xbox 360[24] , in 18.11.2014 for PS4 and Xbox One and in 14.4.2015 it was released on PC, Windows[25].

The game is based on proprietary game engine, called RAGE (Rockstar Advanced Game Engine) [42], which is used as a base for most of Rockstar Games products.

Till the release on Microsoft, Windows, it has been in development for 5 years with approximate 1000-person team [23]. The world of GTA V was modelled on Los Angeles[32] and other areas of Southern California, with road networks respecting design of Los Angeles map.

As could be expected from AAA game like GTA V, motion capture was used to character's both body and facial movements.

There are several reasons why GTA V is better for dataset creation than other games. To use a game for dataset creation, we have multiple requirements. The graphics of the game must be near photorealistic, since we try to use it instead of photos for computer vision tasks. This disqualifies most of games, and leaves us only with AAA games produced by big companies and few other games with State of the Art graphics.

The other requirement is possibility of good-enough way to interact with the game programmatically. Usually we want to setup at least part of the environment before gathering data. This part heavily depends on community around the particular game.

Also the advantage of GTA V compared to some other games is abundance of models and various sceneries in its virtual world. It has complex transportation system of roads, highways, intersections, railroad crossing, tunnels, and pedestrians. It also has urban, suburban, and rural environments [22].

In gaming subculture, there are communities where people specialize in reverse-engineering of games and development of modifications to these games. These people are called modders or mod developers, and these unofficial modifications and extension of games are called mods. For few games, developers welcome this kind of activity and sometimes they even release tools to

ease the game modding. In most cases, the game developers simply don't care and in few cases, they actively fight against the reverse-engineering and modding.

The GTA V is second case, where Rockstar Games does not actively try to prevent the reverse-engineering, but they don't release any tools to ease it, either. This results in cyclic process of Rockstar Games releasing new version of game, including backward compatibility (BC) breaks, and community reverse engineering the new version and adjusting their mods to work with the new version.

The modding community around the GTA V is based mostly on community around GTA IV, which was previous big game produced by Rockstar Games. So many tools are just GTA IV based and only modified to work with GTA V. Luckily, the community is large and productive, so we have many mods and many function in GTA V reverse-engineered and thus prepared for programmatic interactions.

### **3.1.1. Cars**

There is big variety of cars models. Specifically, there are 259 car models, all of them are listed here [5]. These models cars of various shapes and sizes, from golf carts to trucks and trailers. This diversity is representative of real distribution of vehicles. It even allows us to simulate environments with various types of vehicles, which would be very difficult in real environment. GTA V provides us many information about cars, more on this will be covered in section 3.5.

### **3.1.2. Pedestrians**

GTA V has pedestrians and provides some information about them, more on this in section 3.5. The game has pedestrians of both genders and various ethnicities. Pedestrians appear in various poses, like standing, walking, sitting, many animations etc. The main drawback of GTA V is that all pedestrians are about the same height[22].

## **3.2. Automotive Simulators**

Currently, there are some open-source simulation platforms for automotive industry which could be theoretically used for creating synthetic datasets. But compared to AAA games like GTA V, they have much less resources and much less customers to finance the development. In result, simulators have worse graphics than AAA games and NPC (non playable characters) don't have as sophisticated behaviour. In GTA V, drivers mostly follow traffic regulations, traffic lights and traffic lanes, which leads to very realistic environment better than simulators can provide.

## **3.3. GTA V modding ecosystem**

Although the modding community is quite big, as it is in lots of open-source communities, essential part of community depends on one person. Here, it is Alexander Blade. In his free time, he reverse-engineered big part of GTA V and developed ScriptHookV[12], library enabling to perform native calls into GTA V in C++ and develop GTA V mods in C++. Currently, more people in community participates in reverse-engineering and they share their knowledge in GTA forum thread[11].

List of all reverse-engineered native functions is kept in following list [10]. Assumably, GTA V contains ~5200 natives. There is no original native name list of functions in GTA V, name hashes are used instead. During reverse-engineering and game decompilation, ~2600 native names were discovered using brute-force and manual checking afterwards. For these functions, number of parameters and returns of these calls are also known. In the native functions list, for big part of functions we know their name, signature and how do they affect the game. The rest remains to be discovered yet.

When new version of game is released, in few days to weeks, new version of ScriptHookV is released, fixing BC breaks.

Other heavily used mod in community is ScriptHookDotNet2, which is built atop of ScriptHookV and creates bridge between C# language and ScriptHookV, effectively allowing to write GTA V mods in C#. It is available as open-source [18]. Along with creating bridge between C# and GTA V, it wraps most used native calls into classes, leveraging object-oriented paradigm for mod development using getters and setters as proxies for native calls.

Next notable mod is NativeUI[28]. It renders windows atop of GTA V GUI and allows us to define custom control panels for manipulating custom functionality in other mods.

Unlike most of other mods, these three mods act more as a framework for mod development.

Since GTA V is a game, it requires human interaction. For simulator-like behaviour we would want the car to drive autonomously to crawl data without human interaction. This can be done using VAutodrive[20]. This allows us to use NPC automatic behaviour patterns for main player, letting the player randomly wander the world, even in car, without need of human assistance during crawling. Unfortunately, this package is not open-source.

Generally, the community is not united in their view on open-source. Some mods are available open-source on GitHub. Other mods are being distributed only as compiled binaries[2]. Lots of modders develop mostly by trial and error, and no comprehensive documentation for mod development is available, unfortunately. There are some tutorials [56], but they are far from complete and provide only basic knowledge, leaving reader without deeper understanding of underlying principles.

Modders mostly meet online on few GTA forums, where they exchange knowledge [3, 4]. GitHub or Stack Overflow, which are biggest information sources for usual software development, are not used much in GTA modding community. Due to this fact, these forums, along with source code of open-source mods comprise knowledge-base of mod development.

### **3.4. Simulation environment and development stack**

In this thesis, I use mod based on [35] but enhanced to gain more control of the game and to obtain more information from the game.

In later text, I'll refer to some GTA V native functions or data structures which are output of GTA V native functions. To be consistent and to help understanding, I will use function names from native function list [10].

The basic architecture of C# mods come from the ScriptHookDotNet2, where each mod script extends the GTA.Script class. For each child of this class, we can set integer Interval, Tick and KeyUp callbacks. Interval property determines how big interval in milliseconds is between consecutive Tick calls. Tick callback is being called periodically, so here we can set tasks which we want to perform periodically, e.g. screenshot gathering. The KeyUp callback is for interacting with user and reading the user's keyboard input. For data gathering mods, this is mostly used for

debugging purposes, script disabling or restarting.

The ScriptHookDotNet2 brings useful feature for debugging and developing scripts based on in. When changing mod compiled binaries, we don't have to restart the game for newer version of mod to be active. Pressing Insert causes all C# binaries to reload, causing new version of source code to load into game, which dramatically decreases time of feedback loop during development. This does not work for C++ mods and compiled .asi files.

During the data retrieval from the game, two types of data are being gathered. Image data from GPU buffers and data about camera, cars, pedestrians and other in-game entities. All image data are being persistent into the filesystem directly. Other data are persisted into PostgreSQL database running locally on the machine. Since the main mod life-cycle loop is running in single thread, other threads are used for sending data into the database for faster simulation. Other setups are possible, depending on use-case of gathered data and need for scalability. Johnson-Roberson et al. [35] send all images into the Amazon Web Services and save them in a S3 bucket, also the database may run remotely and since the communication with database runs in separate thread, longer delay is not an issue. Other approached are saving all data into the filesystem directly, without database, denormalized per image. This is easier to setup, but leads to complications during data querying, because SQL is much more suited querying tool due to the relational nature of these data.

Since the data retrieval takes many hours usually, there is sometimes need to change some parameters of the environment without stopping the run or to generally control the data retrieval remotely. For this purpose, the mod opens a socket server during startup and reads from it during the Tick method call. Along with the modded game running, there is a python REST based web server with simple controls for changing time of day, weather, stopping and restarting the data retrieval. During the web server startup, it created socket client which connects to the socket server in GTA mod. This setup allows to remotely control the data retrieval over the internet.

The web-server part with socket client is available on <https://github.com/racinmat/GTAVisionExport-Server>. The installation procedure and running is described in the readme. It can be run simply by `python main.py` which starts the server on port 5000. It also contains HTML website with server as a client for the REST API, this can be started either by simply running local Nginx web-server or by using prepared docker container with properly configured server. This is run, as usual docker container, by `docker compose up`. The repository also contains lightweight web-based gallery for browsing gathered images. The main problem with viewing gathered data is their size. Usually there is hundreds of thousands images (RGB image, depth image and stencil image per sample) in single directory, which is difficult to handle for both windows and unix operating systems. To solve this issue, I developed a lightweight REST API based python script with pagination support for viewing this dataset. It can be run by `python gallery.py` which starts the REST server on port 5001. The client side of this paginated gallery is in file `gallery.html` and also uses the Nginx server to run, same as website for controlling the data gathering. It uses HTTPS protocol with self-signed certificate, and the Nginx server is configured to use the HTTP2 protocol which supports large number of requests at the same time. This bypasses the restriction of accessing 6 resources at the same time from one domain which is in HTTP1.1. Thanks to this, hundreds of images can be displayed in very fast manner, both locally and remotely. The gallery can be seen in figure 3.1.

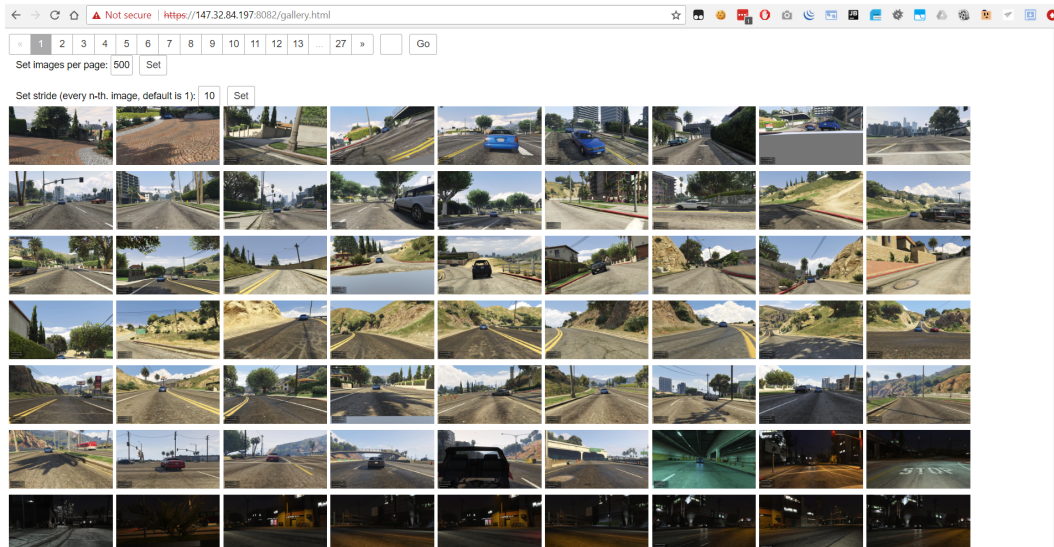


Figure 3.1.: Dataset viewing web interface

### 3.5. GTA V native API and data obtaining

The data obtained from GTA V can be divided into multiple categories.

- Image data
- Rendering pipeline matrices
- GTA V internal data
  - entities
  - camera
  - player
  - other data via API

#### 3.5.1. Image data

There are 3 image data. RGB image, depth image and stencil image.

RGB image is usual camera image. Depth image is content of GPU's depth buffer, in NDC. More detailed description of depth values is in subsection 3.6.3. The last is pixel-wise stencil buffer. The stencil semantics is explained in the next paragraph.

#### Stencil data

Stencil buffer contains auxiliary data per pixel. It is 8bit unsigned integer, where 1.-4. bits (counting from LSB) contain object type ID, and 5.-8. bits contain certain flags.

That means there are 15 object types and 4 flags.

For some object type IDs, I reverse engineered its semantics based on corresponding RGB image.

Object type ID binary	Object type ID decimal	Semantics
0000	0	background (buildings, roads, hills...)
0001	1	pedestrian
0010	2	vehicle
0011	3	tree, grass
0111	7	sky

The background, pedestrian and vehicle IDs are most important for vehicles detection and semantic segmentation, and other object types are not so valuable for these tasks, which is why I didn't investigate further in semantics and they remain to be reverse-engineered.

For stencil flags, semantics was discovered for half of them.

position of bit	position in whole stencil value	Semantics
5	xxx1xxxx	artificial light source
8	1xxxxxxx	player's character

Sample stencil image can be seen in 3.3.

## Extracting images from GPU's internal buffers

To understand how the image gathering works, we need to dive deeper into Microsoft Windows graphics.

In Microsoft Windows, the main graphics engine is DirectX (roughly Windows equivalent of OpenGL). One part of DirectX is Direct3D, which is used to render 3D graphics with hardware acceleration, and most importantly, it provides graphics API. The whole process of obtaining image data is done by mod provided as part of the paper [35]. The mod has two parts, called native and managed plugin.

Image data is being obtained by native plugin by hooking into Direct3D 11's present callback. That means the native call is replaced with custom code, which is being executed and then returns to the native call. In that custom code, content of GPU's buffers is copied. Specifically, the depth and stencil data are captured by hooking into Direct3D's ID3D11ImmediateContext::ClearDepthStencilView and saving the buffers before each call. Because of optimizations applied by the graphics card drivers, the function needs to be re-hooked into the clear function each frame. When saving each sample, the managed plugin requests all current buffers from the native plugin and the buffers are downloaded from the GPU and copied into managed memory.[35].

### 3.5.2. Rendering pipeline data

Direct3D allows us to get rendering pipelines through the D3D11\_MAP\_READ call. This way, the world, world-view, and world-view-projection matrices are obtained. Let's denote them as world matrix =  $W$ , world-view by =  $VW$ , and world-view-projection =  $PVW$ . We need to get individual matrices, which we obtain by multiplication by matrices inversion:

$$V = VW \cdot W^{-1}$$

$$P = PVW \cdot (VW)^{-1} = PV \cdot W^{-1} \cdot V^{-1}$$

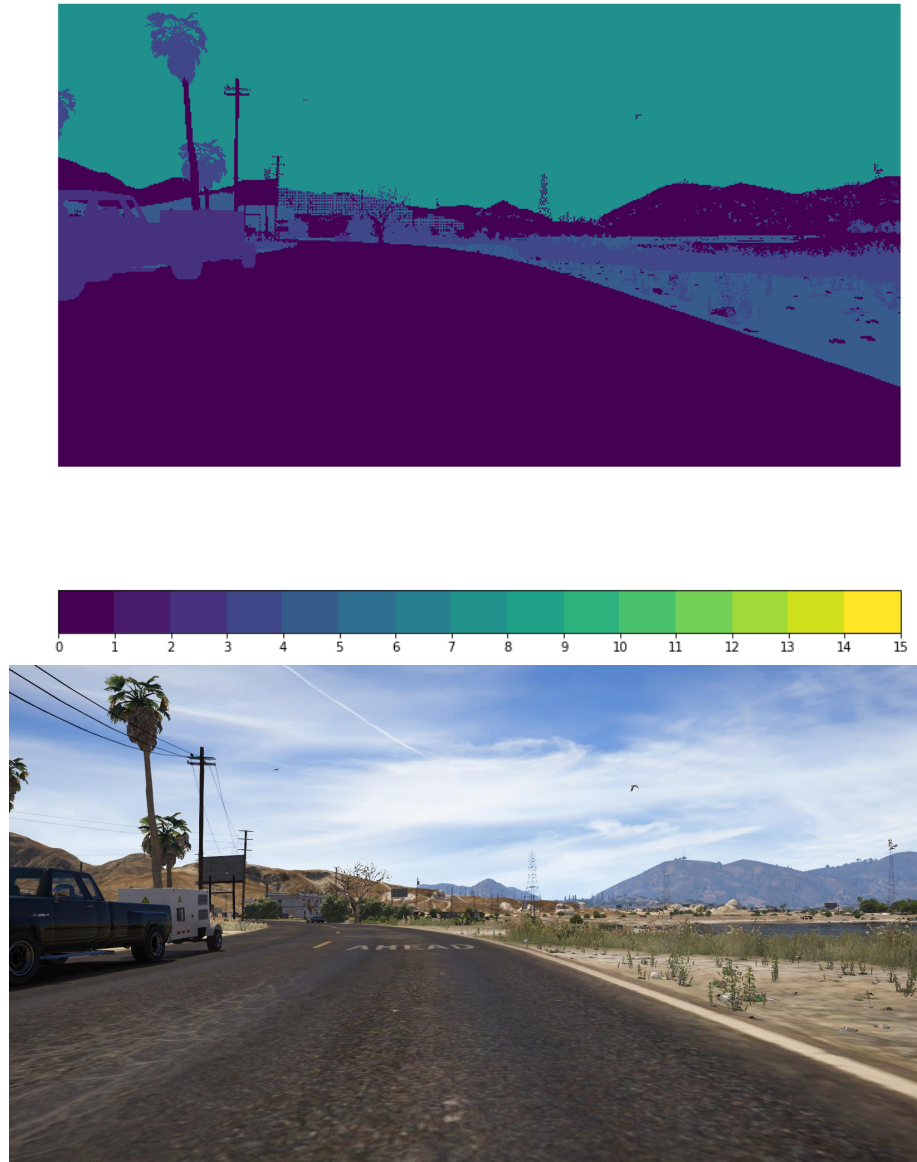


Figure 3.2.: Sample stencil object types image and corresponding RGB image



View and projection matrices are important on their own, without the world matrix. Their semantics and importance is more described in section 3.6. These matrices can be simply obtained by inversion as stated above. But this approach is not numerically stable, and sometimes causes resulting matrix to be incorrect and not usable for further usage. Another caveat of this approach is that during data gathering in higher speeds, the native call becomes laggy and resulting matrices are highly imprecise. Although we can obtain these matrices via the native call, they can be reconstructed with higher precision, as described in 3.6.

### 3.5.3. GTA V internal data

These data are probably most valuable compared to data gathering by other methods. In this section, I describe which data about various game objects can be obtained and how to obtain them.

All data in this section are obtained through native calls into GTA V, which are listed here [10]. As mentioned above, they can be called from C++ and C#. For convenience, and because most of my mod development is done in C#, I will also describe the C# wrappers. The ScriptHookDotNet2[18] wrapper heavily uses object properties. The C# API is divided into multiple classes, listed here. Each class has properties, whose getters and setters are implemented as calling the native functions. This feature is nice tooling and leads to more readable and maintainable code. I will describe parts of API which are most useful for synthetic datasets creation.

#### Coordinate systems and axes

The model, world and view coordinate systems are all in meters. In the model coordinate system, e.g. when we have coordinate system of a car, Z-axis is oriented upwards, Y-axis is oriented in front of the car, and X-axis to the right of the car. In the camera coordinate system, the Z-axis is oriented behind the camera, Y-axis upwards of camera and the X-axis to the left of camera. In the world coordinate system, if the camera has rotation = (0, 0, 0), it is heading in direction of Y-axis, X-axis is heading right of the camera, and Z axis is heading upwards.

#### Game state manipulation

In the ScriptHookVDotNet2, there is Game class, which is the main entry-point for most of game state manipulation. Here I'll describe methods and properties useful and needed for data retrieval.

```
Game.Pause(true)
```

pauses the whole game.

```
Game.Pause(false)
```

un-pauses the game. The

```
Game.ScreenResolution
```

property returns Size object with height and width of the current screen, so

```
Game.ScreenResolution.Width; Game.ScreenResolution.Height;
```

returns screen width and height respectively. As seen above, the main player character can be accessed by `Game.Player.Character` property.

The Player Character property is used for handling the main player. It has following method important for data retrieval. `Game.Player.Character.Position` provides position of player in world coordinates. This is useful if we want to obtain entities only in certain distance of player or if we want to spawn new vehicle on player's position. Similarly to position, we can access player's current velocity by

```
Game.Player.Character.Velocity
```

which returns the velocity 3D vector. If we have a vehicle, we set the player as driver as follows

```
Game.Player.Character.SetIntoVehicle(vehicle,
VehicleSeat.Driver)
```

. When player is in a vehicle, we can access it later by the

```
Game.Player.Character.CurrentVehicle
```

property.

Other important Class is World, which, as seen above, provides the camera handling interface, and many other features. As mentioned above, the `World.DestroyAllCameras()` clears all scripted cameras. The `World.CreateCamera()` creates new scripted camera. The `World.RenderingCamera` holds reference to the currently active scripted camera. Setting the camera to the `World.RenderingCamera` activates that camera and starts rendering with that camera, and setting null reference returns the view to the Gameplay camera, which is default camera used during playing.

Other methods allow us directly manipulate the world. The `World.CurrentDayTime` returns the `TimeSpan` object, which is time in day in the GTA world. By setting this property we can change the time of day as we need by assigning the `TimeSpan` instance

```
World.CurrentDayTime =
new TimeSpan(int hours, int minutes, int seconds)
```

. The `World.Weather` uses same getter, setter interface, so `World.Weather` returns current weather, and `World.Weather = Weather.Foggy` sets the weather to be foggy. List of all possible weathers is in the `Weather` enum, which contains `Unknown`, `ExtraSunny`, `Clear`, `Clouds`, `Smog`, `Foggy`, `Overcast`, `Raining`, `ThunderStorm`, `Clearing`, `Neutral`, `Snowing`, `Blizzard`, `Snowlight`, `Christmas`, `Halloween`.

The World class also contains the

```
World.CreateVehicle(Model model, Vector3 position)
```

which spawn new car in the game and returns reference to the newly spawned car. Position is in world coordinates and model can be any of vehicle models in game. For instance,

```
World.CreateVehicle(new Model(VehicleHash.Seven70),
Game.Player.Character.Position)
```

creates new sports car in player's position . Whole list of known models is available in [https://github.com/crosire/scripthookvdotnet/blob/dev\\_v3/source/scripting/World/Entities/Vehicles/VehicleHash.cs](https://github.com/crosire/scripthookvdotnet/blob/dev_v3/source/scripting/World/Entities/Vehicles/VehicleHash.cs) where 554 model hashes are enumerated.

## Camera

The camera is probably one of the most crucial parts of the API. There is Gameplay Camera, which is the default camera used during usual playing. This camera can be manipulated, but its usage is limited. Other approach is usage of scripted cameras, which can be fully controlled programmatically. We can create multiple scripted cameras and switch between them, but the community discovered there is hard limit of 26 cameras at time[57]. Camera can be created by calling

```
Camera camera = World.CreateCamera(
    new Vector3(x, y, z), new Vector3(x, y, z), float fov);
```

which returns handle to the new camera. The position is in world coordinates in meters. The rotation is in degrees as rotation around particular axis, as in OpenGL engine. In the Aircraft principal axes terminology, the  $(x, y, z)$  rotation vector means  $(pitch, roll, yaw)$  respectively. The fov argument is vertical field of view in degrees. The default value is 50. One can of course call the underlying native functions directly, but this wrapper helps with managing the handles.

All scripted cameras can be destroyed by calling the

```
World.DestroyAllCameras();
```

Switching to the scripted camera can be done by calling

```
camera.IsActive = true;
```

, and switching from this camera to some other by

```
camera.IsActive = false;
```

Right after creating the camera, when we don't to switch to this camera immediately, we need to deactivate it by these two lines of code

```
camera.IsActive = false;
World.RenderingCamera = null;
```

this code ensures that camera is created properly. We don't know precisely, why is this needed, but this is the price for using the closed and reverse-engineered codebase. By calling the

```
camera.IsActive = true;
World.RenderingCamera = camera;
```

scripted camera becomes active and view is switched to this camera. All properties of camera can be set simply by calling setters

```
camera.position = new Vector3(x, y, z);
camera.rotation = new Vector3(y, x, z);
camera.nearClip = distance;
camera.farClip = distance;
camera.FieldOfView = fov;
```

and read by calling getters

```
Vector3 position = camera.position;
Vector3 rotation = camera.rotation;
float distance = camera.nearClip;
float distance = camera.farClip;
float fov = camera.FieldOfView;
```

The near clip and far clip is again in meters. So we can set all needed parameters simply by calling getters and setters. So if we want to use camera, we simply set parameters and then activate it. This creates the static camera.

Sometimes we want the camera to be moving, e.g. when gathering data by driving car. Camera can be attached to any entity by calling

```
camera.AttachTo(entity, new Vector3(x, y, z));
```

the second parameter is relative offset to middle of the attached entity. The offset is in model coordinate system which means its position moves and rotates with attached entity. During dataset gathering, I used this code

```
camera.AttachTo(Game.Player.Character.CurrentVehicle,
new Vector3(0f, 2f, 0.4f));
```

to attach camera to the front part of player's current vehicle. As seen from code, it attaches camera 2 meters in front of car model's centre and 40cm above it, making it effectively sitting on top of the hood of the car. These parameters are taken from [22].

When we have camera attached to the car, we need to update periodically its rotation, otherwise it will be heading the same direction in world coordinates and won't rotate with car it is attached to. So when we have our Tick method, which is being called periodically, we need to update the active camera like this:

```
camera.AttachTo(Game.Player.Character.CurrentVehicle,
cameraPosition);
camera.Rotation = cameraRotation;
```

if we want to have our camera rotated in fixed offset compared to car rotation (e.g. camera looking behind the car), we simply set camera's rotation as offset like this

```
camera.AttachTo(Game.Player.Character.CurrentVehicle,
new Vector3(0f, -2f, 0.6f)); // now our camera is sit-
ting in back of the car
camera.Rotation = Game.Player.Character.CurrentVehicle.Rotation
+ new Vector3(0f, 0f, 180f);
```

which sets camera rotation in world coordinates as a sum of car's rotation and relative rotation of camera, 180° yaw.

## Game entities

All game entities extend the abstract Entity class. Important children of Entity class are Ped, Vehicle and Prop classes, wrapping pedestrians, vehicles, and various objects, respectively. List of all entities contained in the entity pool can be obtained by `World.GetAllEntities()`.  
Methods

```
World.GetAllPeds(); World.GetAllVehicles(); World.GetAllProps();
```

will return list of all pedestrians, vehicles, and props, respectively. These lists are huge and we don't need all of returned entities usually. Most of the time, we are interested only in objects on the screen, which are only in certain distance from us. The most straightforward option is to filter these lists afterwards, but luckily, the library offers us helper methods for filtering the nearby entities more effectively, without need to instantiate more distant entities. These helper methods are

```
World.GetNearbyEntities(Vector3 position, float radius)
```

, and analogously,

```
World.GetNearbyPeds(Vector3 position, float radius);
World.GetNearbyVehicles(Vector3 position, float radius);
World.GetNearbyProps(Vector3 position, float radius);
```

. As expected, radius is in meters, position is in world coordinates. So obtaining for instance all vehicles up to half kilometres distant from the current player, we call

```
World.GetNearbyVehicles(Game.Player.Character, 500.0f)
```

. Every entity has position, rotation, velocity, and handle. Position and rotation have similar semantics as cameras. Velocity is velocity as a 3D vector. The handle is unique in-game identifier of particular entity, allowing identifying it across whole game during data gathering, and lets us identify same entity on multiple images, which is useful for identifying motion of entity through different images. By calling `entity.Model.Hash` on a particular entity, we obtain its hash, which can be used to spawn new entities with same model. For vehicles, there is `entity.ClassType` property, describing type as one of 21 vehicle types. Whole list can be seen in the enum `VehicleClass` in the [https://github.com/crosire/scripthookvdotnet/blob/dev\\_v3/source/scripting/World/Entities/Vehicles/Vehicle.cs](https://github.com/crosire/scripthookvdotnet/blob/dev_v3/source/scripting/World/Entities/Vehicles/Vehicle.cs).

## Gathering data from active camera

In this part, I'll describe how to access data from internal GPU buffers and how to persist these data.

Before we gather buffers contents, we want to pause the game. Since we don't get the data from buffers perfectly synchronized, we pause the game to make sure RGB, depth and stencil buffer contain data coming from same frame. `Game.Pause(true)` pauses the game. The whole data retrieval from buffers is done via `GTAVisionExport` native plugin [35]. When the game is stopped, we can obtain RGB, depth and stencil buffer contents by

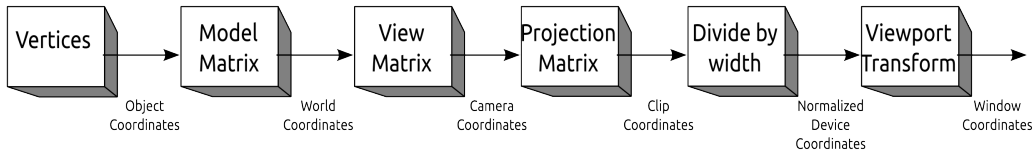


Figure 3.3.: Rendering pipeline

```

var color = VisionNative.GetColorBuffer();
var depth = VisionNative.GetDepthBuffer();
var stencil = VisionNative.GetStencilBuffer();
  
```

and then, we save it to the filesystem as TIFF image. Although TIFF is not the most used format for data, it is able to persist image whose pixels contain float values, which is crucial for depth buffer.

The RGB buffer is usual 8bit unsigned integer RGBA image. The depth buffer contains float values, with 32bits precision, in range from 0 to 1, representing depth value in NDC space. The stencil buffer contains 8bit unsigned integer image.

### 3.6. Reverse-engineering the RAGE rendering pipeline

As mentioned above 3.1, GTA V uses proprietary game engine, Rockstar Advanced Game Engine (RAGE). The basic premise of rendering pipeline is same as in well known graphics engines like OpenGL. The pipeline is shown in figure 3.3. Following section will be discussing mostly computer graphics related problems. Due to some terminology inconsistency between computer graphics and computer vision, all terms used here will be computer graphics related. Probably most confusion here could be caused by projection matrix. In computer vision, projection matrix is projection from 3D to 2D, the matrix reduces dimension. In computer graphics, all coordinates are kept in 4D, in homogeneous coordinates as long as possible. Here the projection matrix represents projection from frustum seen by eye into cuboid space of Normalized Device Coordinates.

In is part, I will describe some transformations between individual RAGE coordinate systems. Some points here will have part of name in lower index. The name of coordinate system will be denoted in upper index. In RAGE there are 6 coordinate systems.

Name	Abbreviation	Example point $x$
Object Coordinates	O	$x^O$
World Coordinates	W	$x^W$
Camera Coordinates	C	$x^C$
Clip Coordinates	L	$x^L$
Normalized Device Coordinates	NDC	$x^{NDC}$
Windows Coordinates	P	$x^P$

Most of points we handle in GTA already are in world coordinates. But some points, like `GAMEPLAY::GET_MODEL_DIMENSIONS` =  $(x_{max}^O \ y_{max}^O \ z_{max}^O) (x_{min}^O \ y_{min}^O \ z_{min}^O)$  output, are in object coordinates. Transitions between adjacent coordinate systems will be demonstrated on model dimensions because it is

on the few vectors which are obtained in Object Coordinates and there is need to project them into Window Coordinates.

### 3.6.1. Object to World Coordinates

To get world coordinates of model dimensions, we use traditional rigid body transformation based on ENTITY::GET\_ENTITY\_ROTATION=  $(\alpha \ \beta \ \gamma)$  Euler angles,

and ENTITY::GET\_ENTITY\_COORDS=  $(x^W \ y^W \ z^W)$ .

Because all coordinates will be homogeneous coordinates, the above-mentioned model dimensions vectors will be transformed to following form  $(x_{max}^O \ y_{max}^O \ z_{max}^O \ 1) (x_{min}^O \ y_{min}^O \ z_{min}^O \ 1)$ .

The transition is represented by model matrix

$$M = \begin{bmatrix} 1 & 0 & 0 & x^W \\ 0 & 1 & 0 & y^W \\ 0 & 0 & 1 & z^W \\ 0 & 0 & 0 & 1 \end{bmatrix} \begin{bmatrix} 1 & 0 & 0 & 0 \\ 0 & \cos(\alpha) & -\sin(\alpha) & 0 \\ 0 & \sin(\alpha) & \cos(\alpha) & 0 \\ 0 & 0 & 0 & 1 \end{bmatrix} \begin{bmatrix} \cos(\beta) & 0 & \sin(\beta) & 0 \\ 0 & 1 & 0 & 0 \\ -\sin(\beta) & 0 & \cos(\beta) & 0 \\ 0 & 0 & 0 & 1 \end{bmatrix} \begin{bmatrix} \cos(\gamma) & -\sin(\gamma) & 0 & 0 \\ \sin(\gamma) & \cos(\gamma) & 0 & 0 \\ 0 & 0 & 1 & 0 \\ 0 & 0 & 0 & 1 \end{bmatrix}$$

$$= \begin{bmatrix} \cos(\beta) \cos(\gamma) & -\cos(\beta) \sin(\gamma) & \sin(\beta) & x^W \\ \sin(\alpha) \sin(\beta) \cos(\gamma) + \cos(\alpha) \sin(\gamma) & \cos(\alpha) \cos(\gamma) - \sin(\alpha) \sin(\beta) \sin(\gamma) & -\sin(\alpha) \cos(\beta) & y^W \\ \sin(\alpha) \sin(\gamma) - \cos(\alpha) \sin(\beta) \cos(\gamma) & \cos(\alpha) \sin(\beta) \sin(\gamma) + \sin(\alpha) \cos(\gamma) & \cos(\alpha) \cos(\beta) & z^W \\ 0 & 0 & 0 & 1 \end{bmatrix}$$

and whole transformation is, as expected

$$M \begin{bmatrix} x_{max}^O & x_{min}^O \\ y_{max}^O & y_{min}^O \\ z_{max}^O & z_{min}^O \\ 1 & 1 \end{bmatrix} = \begin{bmatrix} x_{max}^W & x_{min}^W \\ y_{max}^W & y_{min}^W \\ z_{max}^W & z_{min}^W \\ w_{max}^W & w_{min}^W \end{bmatrix}$$

### 3.6.2. World to Camera Coordinates

The transformation from world coordinates is principally the same, but counter-intuitive in definition of used rotation matrices. It also is rigid body transformation, but rotation is defined differently than we are usually used to in computer graphics. The rotation matrices were reverse engineered as part of this thesis from camera position, rotation and resulting view matrix, this coordinate system is nowhere else documented. The camera position is CAM::GET\_CAM\_COORD=  $(x^W \ y^W \ z^W)$  and the camera rotation is CAM::GET\_CAM\_ROT=  $(\alpha \ \beta \ \gamma)$ .

The transformation is represented by view matrix

$$V = \begin{bmatrix} 1 & 0 & 0 & 0 \\ 0 & \sin(\alpha) & \cos(\alpha) & 0 \\ 0 & \cos(\alpha) & -\sin(\alpha) & 0 \\ 0 & 0 & 0 & 1 \end{bmatrix} \begin{bmatrix} \cos(\beta) & 0 & -\sin(\beta) & 0 \\ 0 & 1 & 0 & 0 \\ \sin(\beta) & 0 & \cos(\beta) & 0 \\ 0 & 0 & 0 & 1 \end{bmatrix} \begin{bmatrix} \cos(\gamma) & \sin(\gamma) & 0 & 0 \\ \sin(\gamma) & -\cos(\gamma) & 0 & 0 \\ 0 & 0 & 1 & 0 \\ 0 & 0 & 0 & 1 \end{bmatrix} \begin{bmatrix} 1 & 0 & 0 & x^W \\ 0 & 1 & 0 & y^W \\ 0 & 0 & 1 & z^W \\ 0 & 0 & 0 & 1 \end{bmatrix}$$

to fit the matrix into page, let us propose following substitutions

$$\cos(\alpha) = c_\alpha, \sin(\alpha) = s_\alpha$$

$$\cos(\beta) = c_\beta, \sin(\beta) = s_\beta$$

$$\cos(\gamma) = c_\gamma, \sin(\gamma) = s_\gamma$$

$$\begin{aligned}
 V &= \begin{bmatrix} c_\beta c_\gamma & c_\beta s_\gamma & -s_\beta & 0 \\ c_\alpha s_\beta c_\gamma + s_\alpha s_\gamma & c_\alpha s_\beta s_\gamma - s_\alpha c_\gamma & c_\alpha c_\beta & 0 \\ c_\alpha s_\gamma - s_\alpha s_\beta c_\gamma & -s_\alpha s_\beta s_\gamma - c_\alpha c_\gamma & -s_\alpha c_\beta & 0 \\ 0 & 0 & 0 & 1 \end{bmatrix} \begin{bmatrix} 1 & 0 & 0 & x^W \\ 0 & 1 & 0 & y^W \\ 0 & 0 & 1 & z^W \\ 0 & 0 & 0 & 1 \end{bmatrix} \\
 &= \begin{bmatrix} c_\beta c_\gamma & c_\beta s_\gamma & -s_\beta & x^W c_\beta c_\gamma + y^W c_\beta s_\gamma - z^W s_\beta \\ c_\alpha s_\beta c_\gamma + s_\alpha s_\gamma & c_\alpha s_\beta s_\gamma - s_\alpha c_\gamma & c_\alpha c_\beta & x^W (c_\alpha s_\beta c_\gamma + s_\alpha s_\gamma) + y^W (c_\alpha s_\beta s_\gamma - s_\alpha c_\gamma) + z^W c_\alpha c_\beta \\ c_\alpha s_\gamma - s_\alpha s_\beta c_\gamma & -s_\alpha s_\beta s_\gamma - c_\alpha c_\gamma & -s_\alpha c_\beta & x^W (c_\alpha s_\gamma - s_\alpha s_\beta c_\gamma) + y^W (-s_\alpha s_\beta s_\gamma - c_\alpha c_\gamma) - z^W s_\alpha c_\beta \\ 0 & 0 & 0 & 1 \end{bmatrix}
 \end{aligned} \tag{3.1}$$

and whole transformation is, as expected

$$V \begin{bmatrix} x_{max}^W & x_{min}^W \\ y_{max}^W & y_{min}^W \\ z_{max}^W & z_{min}^W \\ w_{max}^W & w_{min}^W \end{bmatrix} = \begin{bmatrix} x_{max}^C & x_{min}^C \\ y_{max}^C & y_{min}^C \\ z_{max}^C & z_{min}^C \\ w_{max}^C & w_{min}^C \end{bmatrix}$$

From definition of rotation axes in the rotation matrices, following observation can be made.  $z^C$  represents distance from camera in direction of camera heading, and  $x^C$  and  $y^C$  represent horizontal and vertical position of point relative to camera, respectively. But the view frustum of camera is in opposite direction than  $z^C$  axis, which means the camera “is looking” into negative  $z^C$  coordinates.

### 3.6.3. Camera to NDC

This is the first transformation which is not rigid-body transformation. Because camera sees only frustum, this transformation represents transition from frustum to cuboid in Normalized Device Coordinates. The frustum being projected is specified by near clip, far clip, field of view and screen resolution width and height. Usually, none of these parameters are changing during the game, so the projection matrix is usually the same for multiple scenes during data gathering session. Although all of these parameters can be changed programmatically if needed.

The near clip and far clip of camera can be obtained by `CAM::GET_CAM_NEAR_CLIP=  $n_c$`  and `CAM::GET_CAM_FAR_CLIP=  $f_c$` . Width and height of screen resolution are obtained by `GRAPHICS::_GET_ACTIVE_SCREEN_RESOLUTION= ( $W$   $H$ )` and field of view of camera by `CAM::GET_CAM_FOV=  $\varphi_{VD}$`  in degrees.  $\varphi_{VD}$  in radians will be denoted as  $\varphi_{VR}$ .

The near clip and far clip define planes between which the content is being rendered. Nothing before the near clip and behind the far clip is rendered.

The field of view  $\varphi_{VD}$  is only vertical. Horizontal field of view can be calculated from  $W$  and  $H$  ratio, but currently we don't need it.

There is important observation, the far clip  $f_c$  does not figure in the projection matrix at all. In the projection matrix, only  $n_c$  is used. Far clip used in projection matrix is non-changing value which can not be obtained through Camera native function. By reverse-engineering I calculated the value of this new far clip to be 10003.815, details of this calculation are covered in experiments5.1.



The transformation is represented by projection matrix

$$P = \begin{bmatrix} \frac{H}{W \cdot \tan(\frac{\varphi VR}{2})} & 0 & 0 & 0 \\ 0 & \frac{1}{\tan(\frac{\varphi VR}{2})} & 0 & 0 \\ 0 & 0 & \frac{-10003.815}{n_c - 10003.815} & \frac{-10003.815 \cdot n_c}{n_c - 10003.815} \\ 0 & 0 & -1 & 0 \end{bmatrix} \quad (3.2)$$

So the projection to Clip Coordinates is

$$P \begin{bmatrix} x_{max}^C & x_{min}^C \\ y_{max}^C & y_{min}^C \\ z_{max}^C & z_{min}^C \\ w_{max}^C & w_{min}^C \end{bmatrix} = \begin{bmatrix} x_{max}^L & x_{min}^L \\ y_{max}^L & y_{min}^L \\ z_{max}^L & z_{min}^L \\ w_{max}^L & w_{min}^L \end{bmatrix}$$

The transition between Clip Coordinates and NDC is only division by width, so it is

$$\begin{bmatrix} x_{max}^L & x_{min}^L \\ y_{max}^L & y_{min}^L \\ z_{max}^L & z_{min}^L \\ w_{max}^L & w_{min}^L \end{bmatrix} \circ \begin{bmatrix} \frac{1}{w_{max}^L} & \frac{1}{w_{min}^L} \\ \frac{1}{w_{max}^L} & \frac{1}{w_{min}^L} \\ \frac{1}{w_{max}^L} & \frac{1}{w_{min}^L} \\ \frac{1}{w_{max}^L} & \frac{1}{w_{min}^L} \end{bmatrix} = \begin{bmatrix} x_{max}^{NDC} & x_{min}^{NDC} \\ y_{max}^{NDC} & y_{min}^{NDC} \\ z_{max}^{NDC} & z_{min}^{NDC} \\ 1 & 1 \end{bmatrix}$$

where  $\circ$  is Hadamard product, also known as entry-wise product or element-wise matrix multiplication.

Let us have vector  $\mathbf{x} = [x \ y \ z \ w]^T$  in both coordinate systems,  $\mathbf{x}^L = [x^L \ y^L \ z^L \ w^L]^T$ ,  $\mathbf{x}^{NDC} = [x^{NDC} \ y^{NDC} \ z^{NDC} \ w^{NDC}]^T$ . Then, the relation between Clip Coordinates and NDC can also be expressed by following relationship

$$\mathbf{x}^L = \begin{bmatrix} x^L \\ y^L \\ z^L \\ w^L \end{bmatrix} = \begin{bmatrix} x^{NDC} w^L \\ y^{NDC} w^L \\ z^{NDC} w^L \\ w^L \end{bmatrix} = w^L \begin{bmatrix} x^{NDC} \\ y^{NDC} \\ z^{NDC} \\ 1 \end{bmatrix} = w^L \mathbf{x}^{NDC}$$

The view frustum was now transformed into NDC cuboid. The NDC cuboid has dimensions  $x \in [-1, 1]$ ,  $y \in [-1, 1]$ ,  $z \in [0, 1]$ . The x and y coordinates are intuitive, but the z-axis is reverted, so near clip is being mapped to 1 and far clip is being mapped to 0. The NDC is important because it is coordinate space in which GPU operates and depth is gathered from GPU in NDC. The value of  $z^{NDC} = 0$  usually belongs to sky.

The camera divides the camera space to two half-spaces, in front of camera  $z^C < 0$ , and behind camera  $z^C \geq 0$ . The projection transformation from camera space to NDC space works correctly only for points that belong to half-space  $z^C < 0$ . For every point in camera space, we can easily verify to which half-space it belongs and project only points belonging to the  $z^C < 0$  half-space. If we project points behind the camera,  $z^C \geq 0$  to the NDC space, they will be mapped into the NDC space as if they were in front of camera.

### 3.6.4. NDC to Window Coordinates

This is the last transformation of the rendering pipeline and only in this transformation the dimension reduction happen. So far points have been kept in homogeneous coordinates, but window

coordinates are only 2D, expressing  $x$  and  $y$  coordinates of pixel where point will be rendered. Here, we need only `GRAPHICS::_GET_ACTIVE_SCREEN_RESOLUTION= (W H)` because this transformation depends only on screen width and height.

The transformation matrix is

$$T = \begin{bmatrix} \frac{W}{2} & 0 & 0 & \frac{W}{2} \\ 0 & -\frac{H}{2} & 0 & \frac{H}{2} \end{bmatrix}$$

so the NDC to screen transformation is

$$T \begin{bmatrix} x_{max}^{NDC} & x_{min}^{NDC} \\ y_{max}^{NDC} & y_{min}^{NDC} \\ z_{max}^{NDC} & z_{min}^{NDC} \\ 1 & 1 \end{bmatrix} = \begin{bmatrix} x_{max}^P & x_{min}^P \\ y_{max}^P & y_{min}^P \end{bmatrix}$$

Due to the division by width, the pipeline unfortunately can not be expressed as matrix multiplication by matrix constant for all points in one scene.

### 3.7. VirtualScapes Dataset proposal

As part of my thesis, I propose two novel synthetic datasets. Both of these datasets are outdoor, taken from virtual car. Both of these datasets contain outdoor images in all parts of day, dawn, day, evening, and night. They contain most of data described above, to provide as much information as possible for usability in various tasks. Both of these datasets contain full HD RGB-D images, stencil images, position and rotation of camera, positions, rotations, identifiers and types of cars and pedestrians around the camera, projection and view matrix for aligning data between different images.

The first dataset, named Closed VirtualScapes, was used for voxel map reconstruction. It contains images from 4 virtual cameras attached to driving car, placed in circle opposite to each other, mapping space in front of car to create its detailed 3D reconstruction. There are 8371 scenes, each taken from 4 cameras. During this dataset gathering, 13059 meters were driven in virtual world.

The second dataset, named Open VirtualScapes, is demonstration of common automotive dataset from driving car. Compared to real-world datasets, this one has advantage of pixel-wise depth, precise on all surfaces and even in high distances, outperforming LiDAR technology in accuracy and depth point density. It is directly aligned with pixels of RGB images. The datasets consists of 22285 scenes, every of them captured by 4 cameras attached to car, heading different direction, as seen in figure 3.8 where camera positions are marked by white cubes. During this dataset gathering, 34340 meters were driven in virtual world. Both datasets are publicly available and can be downloaded from [http://ptak.felk.cvut.cz/public\\_datasets/GTA\\_V/dataset-website/](http://ptak.felk.cvut.cz/public_datasets/GTA_V/dataset-website/).

To demonstrate possibilities of synthetic, automatically annotated datasets, here are some sample images obtained using my data extraction described in 3.5 . The dataset contains position, rotation, model sizes, identifier and the pixel-wise class segmentation of each car. With this data, I was able to do the 3D and 2D bounding boxes extraction, pixel-wise object segmentation and trajectory tracking. All of these images are part of the VirtualScapes dataset and can be automatically reconstructed using annotations included in dataset.



Figure 3.4.: 3D bounding box - night



Figure 3.5.: 3D bounding box - day

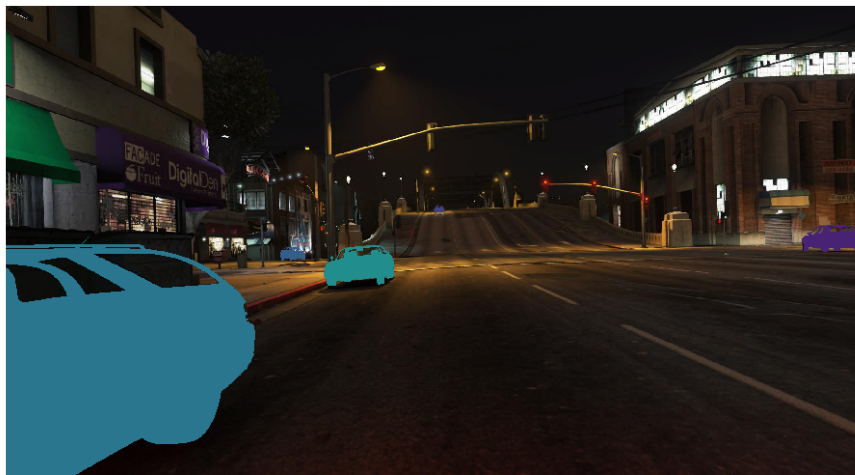


Figure 3.6.: pixel-wise annotation of cars



Figure 3.7.: individual car trajectories



Figure 3.8.: Camera positions for second dataset

## 3D MAP ESTIMATION

When thinking of 3D map estimation, we can utilize the similarity between 3D map estimation and the depth estimation, because in depth estimation, we predict the distance of nearest object pixel-wise, and in 3D map estimation, we have multiple depth levels per pixel and estimate occupancy per each depth level. The neural network output is cuboid with size of  $X \times Y \times Z$  neurons, hence it is useful to represent 3D map of a cuboid as a voxel map with  $X$  width levels,  $Y$  height levels and  $Z$  depth levels. Then we can estimate occupancy per voxel, in other words, per each neuron output. Thus we can represent both depth and 3D map estimation as similar instances, depth estimation being multi-class occupancy classification per pixel where classes are depth bins, and 3D map estimation being occupancy classification per voxel, where we predict occupancy for each voxel.

### 4.1. TensorFlow

In the neural networks research, one of the important factors is the ability to easily and efficiently prototype new architecture and train neural network. TensorFlow [7] is a framework for developing and training neural networks, developed by Google Inc. It is based on declarative programming and the API provides a way to describe the computational graph. This graph is can be then queried for value of any node in the graph given specific input. Other advantage of TensorFlow is almost seeming-less transition between running the calculation graph on CPU and on GPU which allows to users to describe abstract mathematical operations without the need of low-level optimizations of calculations on CUDA, everything is taken care of by TensorFlow. As a powerful tool for introspections of neural network training, TensorBoard was developed as a visualization utility for TensorFlow. During the training, certain parameters can be logged periodically and then visualized in TensorBoard, enabling visualization of cost function, metrics, input and output images, or weight histograms in time, which leads to more intuitive understanding of issues during solving problems with neural networks training.

### 4.2. Depth estimation

As a task preceding the 3D map estimation, I firstly trained neural network for depth estimation. There are many datasets for depth estimation, but most of them are either indoor with relatively precise ground truth depth or outdoor with sparse depth labels, like in KITTI dataset [26], or

they are in relatively low resolution and loss accuracy in higher distance [47], which is natural for real-world depth measurement. For training, I use Closed VirtualScapes dataset, synthetic dataset gathered from GTA V, described in section 3.7.

This dataset is already in the form of corresponding RGB and depth images, but the depth is in the NDC space so it must first be pixel-wise transformed into the camera view space where the depth is in meters. We might train network directly in the NDC space, but the depth reconstruction learned would be deformed. The NDC space is not linearly mapped into the camera view space, in fact, it is mapped hyperbolically, according to the visualization pipeline [8]. After obtaining the depth in meters, I performed depth binning to obtain the depth representation for the classification task. Since these data are outdoor, the depth varies from 1 meter to 10km, which is the camera far clip and nothing after 10km is rendered. Which is still much bigger depth range than in real world datasets. Depth estimation of very distant objects is harder than for close ones, mainly because their relative size on the image is lot smaller, but also small difference in image can mean big depth difference in meters. And in most of applications, we are interested only in relatively near objects depth estimation. This is why the depth range to 50 meters has been used for binning into 100 depth levels, and one additional depth level was used as the “another” class, depth out of the range, so network would still classify far away pixels as some bin and wouldn’t try to assign them some nearer depth level. This is why there are 101 channels in the network output. Due to this setup, ground truth depth which is used as the correct label during training, has all pixels more distant than 50 meters belong to the same depth class. This is important for visual evaluation of predicted depths.

In convention in neural networks for image processing each layer has usually 4 dimensions. Those dimensions have semantics (batch size, image height, image width, number of channels). The batch size is usually omitted in most of notations because it is constant in all network. Other dimensions change its size in individual layers.

The basic architecture for depth estimation is based on Li et al. [41], but there are modifications. The whole network can be seen in figure 4.1. The input is  $320 \times 240$  RGB image. Bigger images are resized to this size. The overall architecture and individual parameters should be visible in the figure. In each box, the first row is the type of neural network layer, other rows specify either its parameters, or next layer. Conv means convolutional layer, next row after it specifies its parameters, namely kernel, size of last dimension (also sometimes called number of channels), stride, and activation function. For instance, in the second box, second row, “7x7, 64, 2, relu” means 7x7 kernel, last 64 output channels, stride 2 and Rectified Linear Unit activation function. When no activation function is specified, there is no activation function and convolutional layer output is directly input to the consecutive layer. Most of the network consists of two types of block. Resize blocks and non-resize blocks. The naming comes from the property of convolutional layers, specifically the stride parameter. When the stride is 1, width and height dimensions remain unchanged, but when the stride is higher, the width and height are resized. These blocks are the main building blocks of the ResNet network [30] and we can see the layers for residual mapping in non-resize blocks. Non-resize blocks are stacked onto each other multiple times, which is denoted in the figure, specifically non-resize blocks are repeated 2, 7, 35 and 2 times, respectively. As depicted in the figure, output of all blocks from the second resize block onwards are then concatenated together in the channel dimensions, which allows utilization of low-level, mid-level and high-level feature in the last layers of the network. The input layer is denoted by the green background, output layer by blue background, and orange and yellow backgrounds represent layers with dilated convolution. Orange background is used for blocks whose convolution layers uses dilution in rate 2, which means neighbouring neurons

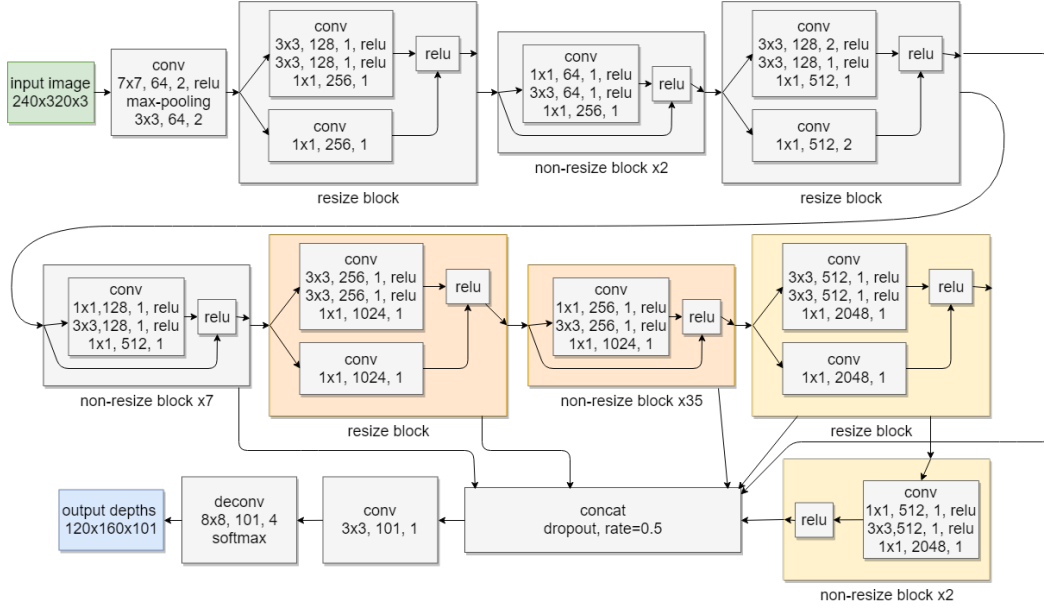


Figure 4.1.: Depth estimation neural network

in the convolution mask have distance=2 from its neighbours, every second neuron is omitted in each direction. The similar property holds for blocks with yellow background, where the dilated convolution has rate 4, which means neighbouring neurons in the convolution mask are 4 neurons distant from each other in the previous layer.

Layers of network which have same architecture as ResNet-152 have been initialized by trained ResNet network. For remaining parameters the following holds. Weights of neuron inputs have been initialized by Xavier initialization from normal distribution, and biases have been initialized to the constant value 0.1. After each layer, the batch normalization has been used, with  $\epsilon = 10^{-3}$  and decay= 0.9997. During the training, the cost is optimized, but it is hard to compare results when different cost is tried only based on visual perception, which is why other metrics are being used for evaluation the accuracy of trained network. For depth estimation, following metrics are reported. Accuracy under threshold, mean relative error, root mean squared error, mean squared log error, and average  $\log_{10}$  error. All of them are calculated pixel-wise. They are formally defined as follows.

1. Accuracy under threshold  $aut(\tau) = \frac{1}{K} \sum_{i=1}^K 1 \left\{ \max \left( \frac{d_i^*}{d_i}, \frac{d_i}{d_i^*} \right) < \tau \right\}$

2. Mean relative error  $rel = \frac{1}{K} \sum_{i=1}^K \frac{|d_i^* - d_i|}{d_i^*}$

3. Root mean squared error  $rms = \sqrt{\frac{1}{K} \sum_{i=1}^K (d_i^* - d_i)^2}$

4. Root mean squared log error  $rmslog = \sqrt{\frac{1}{K} \sum_{i=1}^K (\log_{10}(d_i^*) - \log_{10}(d_i))^2}$



$$5. \text{ Average } \log_{10} \text{ error } \logerr = \frac{1}{K} \sum_{i=1}^K |\log_{10}(d_i^*) - \log_{10}(d_i)|$$

where  $d_i$  is predicted depth on  $i$ -th pixel,  $d_i^*$  is the ground truth depth on  $i$ -th pixel,  $K$  is the total number of pixels per sample, and  $\tau$  is the threshold for accuracy under threshold. The most frequent value is  $\tau = 1.25$ , and this is also used during evaluations of this thesis. Other frequently used values are  $\tau = 1.25^2$  and  $\tau = 1.25^3$ .

### 4.3. 3D map estimation

The 3D map estimation from single RGB image is an abstract task and has many possible representations. In many tasks, voxel-map has proven to be good representation of the 3D space. Voxel (volumetric pixel) is the smallest distinguishable unit in 3D space, it is 3D analogy of 2D pixel. In this scenario, each voxel has one of three states: free, occupied and unknown. The size of voxel is not generally set and is being chosen to fit particular task. Too big voxel size causes high loss of information, and too small voxel size leads to high amount of voxels, more complicated manipulation with the resulting voxelmap and higher size when persisting the voxelmap.

Image which is used as an input for 3D map estimation is representing only a frustum in 3D map and does not contain information about space outside of this frustum. Because of this fact, setup in this thesis focuses only on reconstruction of 3D space inside the frustum viewed by the camera taking the image. Output of the neural network is  $X \times Y \times Z$  cuboid, which will be mapped to the frustum so output of each neuron represents point in the frustum. Mapping between the the cuboid and frustum is contained in the projection matrix 3.6.3 which is used for the training dataset creation and for reconstruction of pointcloud from neural network output during prediction. With this setup, the model is predicting occupancy of points sampled from the frustum. In my setup, the frustum will be up to 25m from camera.

#### 4.3.1. Training dataset construction from depth images

The synthetic dataset created from GTA V contains depth images and camera parameters, so there is need to reconstruct the 3D map and sample it to create the training dataset. For 3D map reconstruction, I gathered data from four cameras with positions relative to the driving car, as seen in figure X where each white cube represents camera position 4.2. Totally there are 4 cameras, equally placed on the circle with 8 meters circumference. This setup will demonstrate the whole process of building 3D frustum map from 4 cameras.

From these 4 cameras, I gathered 4 RGB and depth images, shown in figures 4.3 and 4.4. I also gathered camera parameters, namely position, rotation, near clip, and field of view. With these parameters, depth images can be easily transformed into the pointcloud in world coordinate system. Let us have  $I^1$  depth image from the 1st camera with with width  $W$  and height  $H$  pixels. Since depth image contains value in NDC space then,  $I^1 = (d_{i,j}) \in [0, 1]^{W \times H}$  holds, where  $d_{i,j}$  is value of pixel with coordinates  $[i, j]$ . For every pixel, we know its depth value and coordinates in the pixel space, thus we can describe it as a point in NDC space

$$\mathbf{x}_{i,j}^{NDC} = \begin{bmatrix} x^{NDC} \\ y^{NDC} \\ z^{NDC} \\ 1 \end{bmatrix} = \begin{bmatrix} \frac{2i}{W} - 1 \\ -\left(\frac{2j}{H} - 1\right) \\ d_{i,j} \\ 1 \end{bmatrix}$$



Figure 4.2.: Camera positions for 3d reconstruction



Figure 4.3.: extracted RGB images from 4 cameras

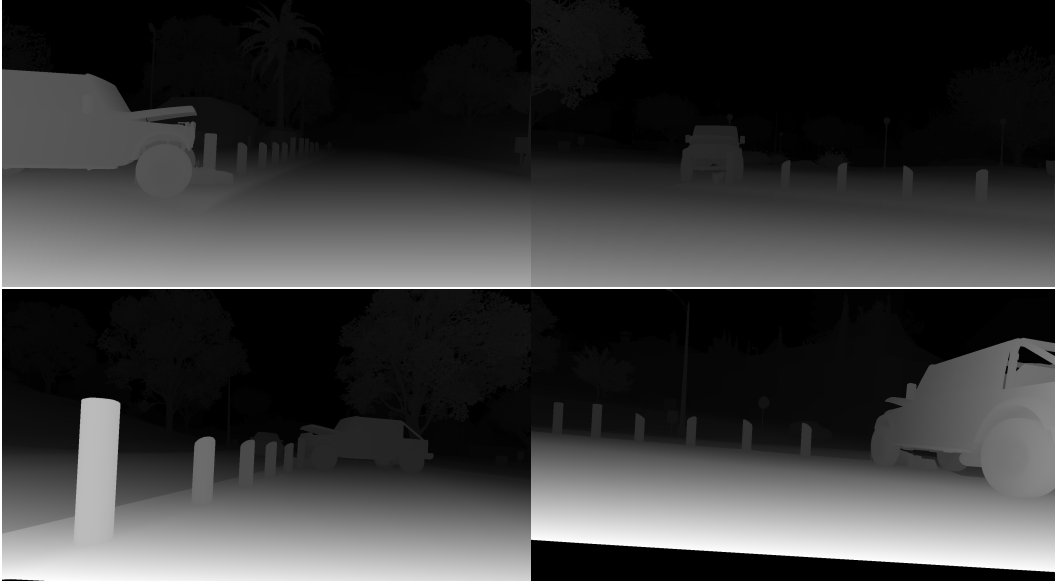


Figure 4.4.: extracted depth images from 4 cameras

, where the  $x_{i,j}^{NDC}$  is pixel $[i, j]$  transformed into NDC space. The sign change in  $y^{NDC}$  is caused by indexing conventions of images, where lowest pixel height is in the upper part of image but in NDC space, lowest  $y^{NDC}$  value is in the lower part of image. This holds because  $x^{NDC}, y^{NDC} \in [-1, 1]$ . With this pixel-wise transformation, we can transform each depth image  $I^k, k \in 1..4$  into pointcloud in NDC  $P_k^{NDC}$ . By using transformation matrices described in 3.6.2 and 3.6.3 we can transform these pointclouds from different cameras into the same world coordinate space. Let us have  $P$  matrix from 3.2 and  $V_k$  matrix from 3.1 denoting the view matrix of  $k$ -th camera, since these matrices are regular, we can do the transformation

$$P_k^W = V_k^{-1} P^{-1} P_k^{NDC} \forall k \in 1..4$$

. Then, all pointclouds are merged into one pointcloud  $P^W$  of whole scene seen from 4 cameras

$$P^W = \bigcup_{k \in 1..4} P_k^W$$

. The resulting pointcloud can be seen in figure 4.5. In this setup, all images are nearly Full HD, specifically  $1920 \times 1057$ . This leads to pointcloud of size  $1920 \cdot 1057 = 2029440 \approx 2M$  points. Most of these points are near camera, in unnecessarily high density for this application. To decrease the size of pointclouds and the time to process, them I clustered them into 12cm big voxels and sampled only 1 point per voxel. This sub-sampling decreases the pointcloud size from  $\sim 2M$  points into  $\sim 80k$  to  $\sim 120k$  points, which is 4% to 6% of original size. This sub-sampling is performed per depth image so we can easily link each point in pointcloud with camera it is seen from which is crucial for building occupancy voxelmap. The far clip is over 10000 5.1 and thus the maximum distance from camera is over 10km. For reconstruction of view frustum to 25m from camera, this is unnecessarily large and makes further calculation complicated which is why all depth levels further than 30m were projected into 30m distance before further transformed into pointcloud. This transformation does not affect the space near camera but lowers space needed for representation of the pointcloud during the voxelmap occupancy calculation. Merged

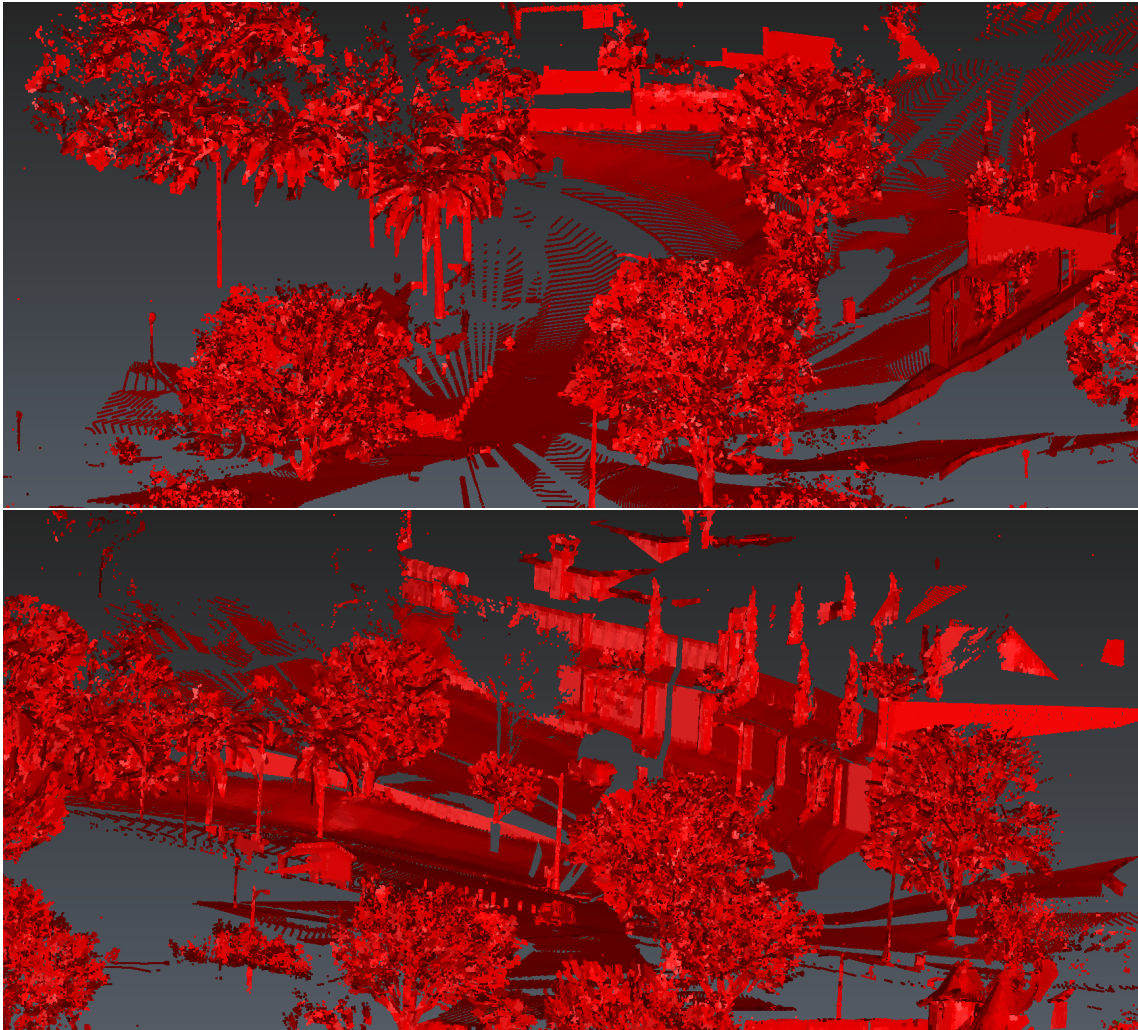


Figure 4.5.: Merged pointcloud from all cameras

pointcloud after projecting distant points into the 30m distance from their camera can be seen in figure 4.6 where I compare pointclouds before and after aforementioned sub-sampling.

After this projection and sub-sampling, I have everything prepared for building a occupancy voxelmap . Voxels in this setup are 25cm big, and each voxel is marked either as occupied, free, or unknown. The resulting occupancy voxelmap is depicted in figure 4.7. The last part of the processing is the sampling of the view frustum from this occupancy voxelmap. This is directly mapped to the output of the neural network. Source code with implementation of the processing pipeline is available at <https://github.com/racinmat/GTAVisionExport-postprocessing>.

### 4.3.2. Metrics and network setup

Although the 3D map estimation is similar to the depth estimation by the problem setup, it is more difficult since we try to infer occupancy of occluded voxels, which was not an issue in depth prediction. Similarly to the depth predictions, metrics for comparing different models and optimizations of different loss functions are used. Compared to the depth estimation where

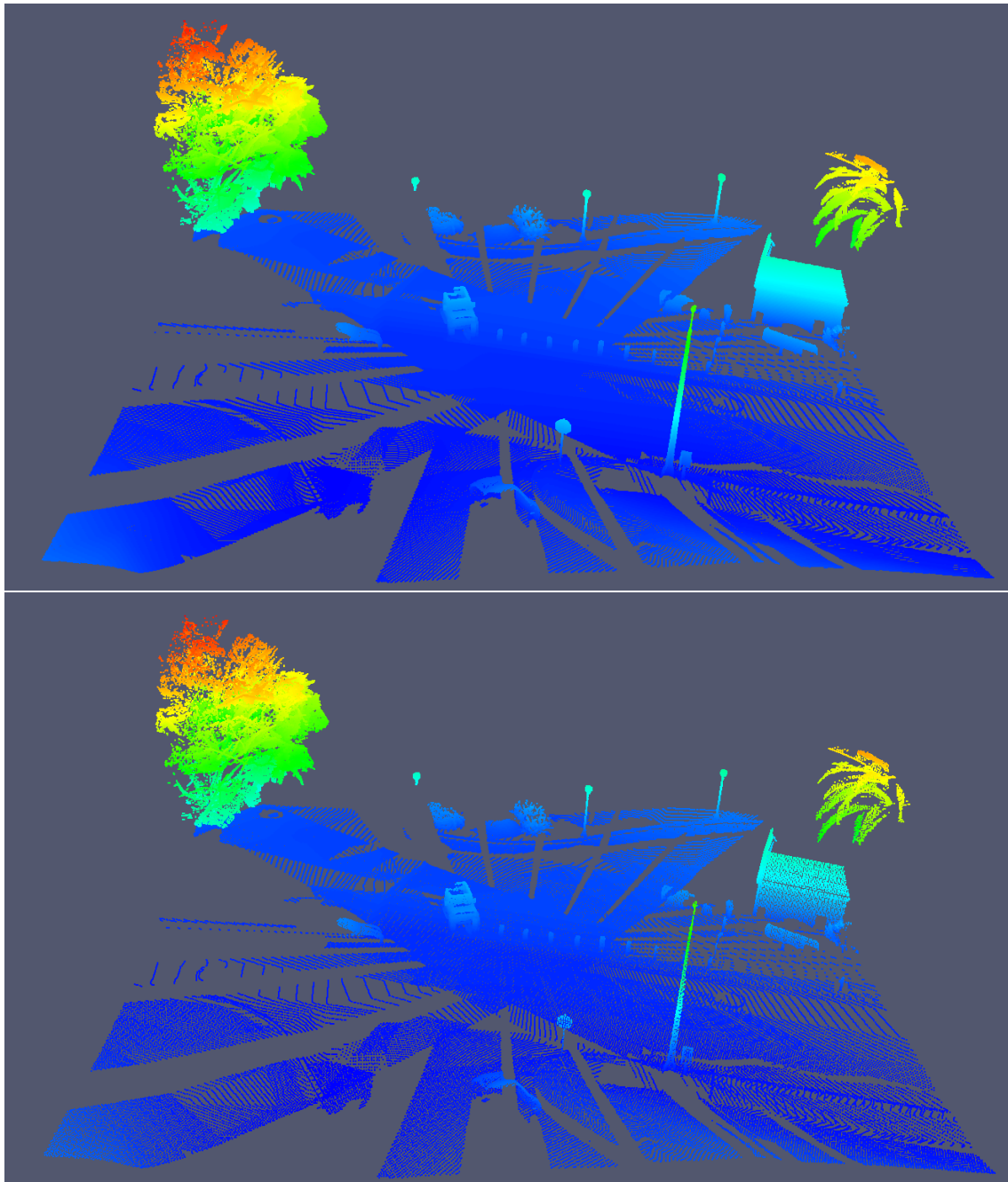


Figure 4.6.: Pointcloud before and after sub-sampling

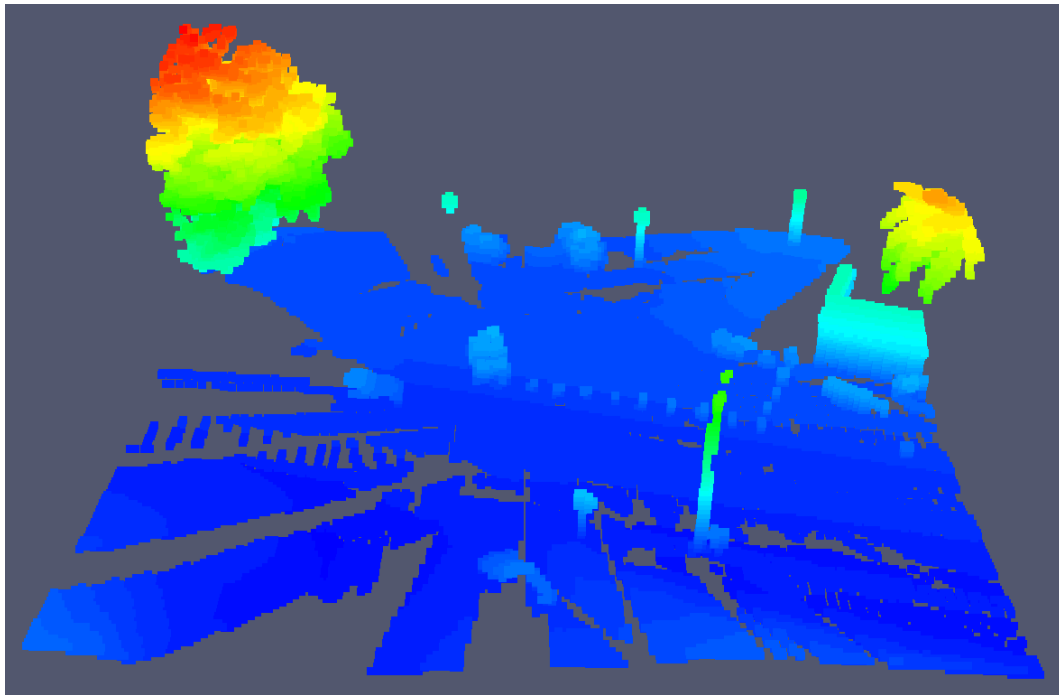


Figure 4.7.: Occupied voxels in occupancy voxelmap

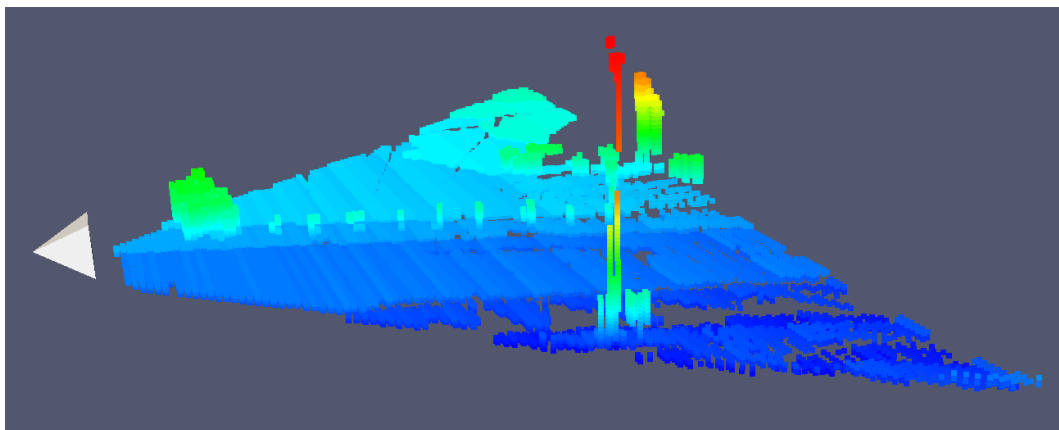


Figure 4.8.: Occupied samples in frustum. Camera is shown by white tetrahedron.

metrics were being calculated on images and based on difference between predicted and ground truth depth, for 3D map estimation the classification based metrics are used since this problem is by definition classification problem.

In this setup of voxel-wise classification, we have 3 classes. Occupied, free, and unknown voxels. Even for the setup of synthesizing 3D occupancy grids, occupancy of some voxels is unknown. For instance, this happens for car interior, occluded when viewed from all cameras and for space below the road. During both training and validation, only known voxels are used for loss calculation and metrics calculation. Let us recapitulate usual terms used for classification problems with respect to this particular problem. Voxel is false positive, if it is classified as obstacle, but is free in ground truth. True positive voxel contains obstacle in ground truth and is correctly classified as an obstacle. True negative voxel is voxel without obstacle, a.k.a free voxel in ground truth classified as free voxel in the prediction. And false negative voxel is free in ground truth and in prediction. So number of voxels in individual categories, which is then used in metrics, can be expressed as

	obstacle in ground truth	free in ground truth
obstacle in prediction	$tp = \sum_{i=1}^K 1 \{obst(M_i) \wedge obst(M_i^*)\}$	$fp = \sum_{i=1}^K 1 \{obst(M_i) \wedge free(M_i^*)\}$
free in prediction	$fn = \sum_{i=1}^K 1 \{free(M_i) \wedge obst(M_i^*)\}$	$tn = \sum_{i=1}^K 1 \{free(M_i) \wedge free(M_i^*)\}$

where  $obst(\cdot)$  is true for occupied voxels and  $free(\cdot)$  is true for free voxels.

Following metrics are used:

1. False positive rate  $fpr = \frac{fp}{fp+tn}$
2. True positive rate  $fpr = \frac{tp}{fn+tp}$
3. Intersection over union  $iou = \frac{\sum_{i=1}^K 1 \{obstacle(M_i) \wedge obstacle(M_i^*)\}}{\sum_{j=1}^K 1 \{obstacle(M_j) \vee obstacle(M_j^*)\}}$
4. L1 distance on known voxels  $dist = \sum_{i=1}^K 1 \{known(M_i^*)\} \cdot |M_i - M_i^*|$

where  $M_i$  is  $i$ -th voxel in predicted voxelmap  $M$ ,  $M_i^*$  is  $i$ -th voxel in ground truth voxelmap  $M^*$ ,  $K$  is number of voxels in voxelmap,  $known(\cdot)$  is predicate true for free or obstacle voxels.

Also the loss function is different from depth estimation. The weighted logistic loss is used. This is voxel-wise, because there can be multiple occupied voxels per pixel and thus does not make sense to use the loss function from depth estimation. The loss function is same as in Zimmermann et al. [61] and is as follows

$$L = - \left[ \sum_{i=1}^K w_i \log (1 + \exp \{-M_i M_i^*\}) \right] \quad (4.1)$$

where  $M_i$  is value of  $i$ -th voxel in predicted voxelmap,  $M_i^*$  is value of  $i$ -th voxel in ground truth voxelmap and  $w_i$  is weight of  $i$ -th voxel. The value of voxel in ground truth voxelmap is as follows:  $M_i^* = 1$  for voxels with obstacles,  $M_i^* = -1$  for free voxels. The weight  $w_i$  serves two

purposes. The first purpose is masking out unknown voxels. The second purpose is to solve the imbalanced classes issue. There are more free voxels than occupied voxels, thus minimizing the sum per all voxels would lead to favouring more frequent voxels. In this case, that would be free voxels and thus it could learn to ignore some obstacles. The weighting modifies the loss so all weights sum to 1 and weights per each class sum to  $\frac{1}{2}$ . The weight  $w_i$  for  $i$ -th voxel is defined as follows.  $w_i = 0$  if  $i$ -th voxel in ground truth is unknown.  $w_i = \frac{1}{2 \cdot \#free\ voxels}$  if  $i$ -th voxel is free and  $w_i = \frac{1}{2 \cdot \#occupied\ voxels}$  if  $i$ -th voxel is occupied.

The implementation of the neural network is publicly available at <https://github.com/racinmat/depth-voxelmap-estimation>.



## EXPERIMENTS

### 5.1. Reverse engineering the true Far Clip

For reverse engineering the far clip, I gathered 33293 screenshots with parameters for projection matrix reconstruction and projection matrices. Because during whole data gathering none of the parameters used to reconstruct projection matrix, was changed, the projection matrix should be same for all records. As mentioned in 3.6.3 parameters for reconstructing the Projection matrix are near clip, far clip, screen width, screen height and field of view.

The screenshot contain both RGB images and depth buffer from GPU.

The projection matrix transforms frustum into cuboid. Open frameworks have publicly available projection matrices, but RAGE does not have publicly available any information about projection matrix, so in order to obtain true far clip, I needed to reverse-engineer the mathematical description of the projection matrix. For approximate estimation of projection matrix parameters, I used DirectX projection matrix[8] as a starting point for analysis, because GTA V requires DirectX, so I assumed it is underlying framework of RAGE.

The DirectX projection matrix is

$$P^{DirectX} = \begin{bmatrix} \frac{2n}{r-l} & 0 & -\frac{r+l}{r-l} & 0 \\ 0 & \frac{2n}{t-b} & -\frac{t+b}{t-b} & 0 \\ 0 & 0 & \frac{f}{f-n} & -\frac{fn}{f-n} \\ 0 & 0 & 1 & 0 \end{bmatrix}$$

where  $n$  is near clip,  $f$  is far clip,  $l$  and  $r$  determine distance between left and right planes of the frustum and  $t$  and  $b$  determine distance between top and bottom planes.

The view frustum is symmetric, so  $r = -l$  and  $t = -b$  [8]. In that case, the projection matrix is simplified to form

$$P^{formal} = \begin{bmatrix} \frac{2n}{r+r} & 0 & -\frac{r-r}{r+r} & 0 \\ 0 & \frac{2n}{t+t} & -\frac{t-t}{t+t} & 0 \\ 0 & 0 & \frac{f}{f-n} & -\frac{fn}{f-n} \\ 0 & 0 & 1 & 0 \end{bmatrix} = \begin{bmatrix} \frac{n}{r} & 0 & 0 & 0 \\ 0 & \frac{n}{t} & 0 & 0 \\ 0 & 0 & \frac{f}{f-n} & -\frac{fn}{f-n} \\ 0 & 0 & 1 & 0 \end{bmatrix}$$

The DirectX maps near clip to 0 and far clip to 1, but from data, where obviously 5.2 nearer pixels had higher value in depth buffer than pixel more far from camera, I concluded that near



Figure 5.1.: Example of RGB image



Figure 5.2.: Example of depth buffer

and far clip are being mapped to 1 and 0, respectively. The far clip being mapped to 0 can also be deduced by pixels for sky having 0 value.

Due to this fact, we switch the near and clip in the matrix formal description

$$P^{formal} = \begin{bmatrix} \frac{f}{r} & 0 & 0 & 0 \\ 0 & \frac{f}{t} & 0 & 0 \\ 0 & 0 & \frac{n}{n-f} & -\frac{fn}{n-f} \\ 0 & 0 & 1 & 0 \end{bmatrix}$$

The example in 5.2 does not have actual depth buffer values, but instead, it is rescaled visualization. Since the depth buffer pixels are in range  $[0, 1]$  and PNG images take unsigned 8bit integer, this image is mapped linearly from  $[0, 1]$  to  $[0, 255]$ . Since even the nearest pixels were distant from near clip and real range of pixels in this image was  $[0, 19]$ , I rescaled it 10 times to range  $[0, 190]$ , so the depth is visible.

At first, I assumed the camera near clip and far clip obtained by native calls 3.6.3 and the projection matrix is same as in DirectX.

The near clip and far clip calculation can be demonstrated on image 5.1.

By calling `CAM::GET_CAM_NEAR_CLIP=  $n_c$`  and `CAM::GET_CAM_FAR_CLIP=  $f_c$`  I obtained values  $n_c = 1.5$  and  $f_c = 800$ . I also obtained projection matrix calculated by method described in 3.5.2, which is

$$P^{real} = \begin{bmatrix} 1.210067 & 0 & 0 & -0.000004 \\ 0 & 2.144507 & 0 & 0.000002 \\ 0 & 0 & 0.00015 & 1.500225 \\ 0 & 0 & -1 & 0 \end{bmatrix}$$

In the formalization of the matrix,  $P_{formal}$ , there are 4 variables.  $r$  and  $t$  appear only in one element of matrix, so they can be verified only after reverse engineering the far clip. From the  $P_{2,2}^{formal}$  and  $P_{2,3}^{formal}$ , I can calculate the near and far clip by

$$\begin{aligned} P_{2,2}^{formal} &= \frac{n}{n-f} \\ nP_{2,2}^{formal} - fP_{2,2}^{formal} &= n \\ \frac{n(P_{2,2}^{formal} - 1)}{P_{2,2}^{formal}} &= f \\ P_{2,3}^{formal} &= -\frac{fn}{n-f} \\ P_{2,3}^{formal}(n-f) &= -fn \\ nP_{2,3}^{formal} &= f(P_{2,3}^{formal} - n) \\ \frac{nP_{2,3}^{formal}}{(P_{2,3}^{formal} - n)} &= f \end{aligned}$$

$$\begin{aligned}
\frac{nP_{2,3}^{formal}}{(P_{2,3}^{formal} - n)} &= \frac{n(P_{2,2}^{formal} - 1)}{P_{2,2}^{formal}} \\
P_{2,3}^{formal} P_{2,2}^{formal} &= (P_{2,2}^{formal} - 1)(P_{2,3}^{formal} - n) \\
\frac{P_{2,3}^{formal} P_{2,2}^{formal}}{P_{2,2}^{formal} - 1} &= P_{2,3}^{formal} - n \\
P_{2,3}^{formal} - \frac{P_{2,3}^{formal} P_{2,2}^{formal}}{P_{2,2}^{formal} - 1} &= n \\
-\frac{P_{2,3}^{formal}}{P_{2,2}^{formal} - 1} &= n \\
\frac{\left(-\frac{P_{2,3}^{formal}}{P_{2,2}^{formal} - 1}\right)(P_{2,2}^{formal} - 1)}{P_{2,2}^{formal}} &= f \\
-\frac{P_{2,3}^{formal}}{P_{2,2}^{formal}} &= f
\end{aligned}$$

From these calculations, we can calculate near and far clip as

$$\begin{aligned}
n &= -\frac{P_{2,3}^{formal}}{P_{2,2}^{formal} - 1} = -\frac{1.500225}{0.00015 - 1} = 1.500225 \\
f &= -\frac{P_{2,3}^{formal}}{P_{2,2}^{formal}} = -\frac{1.500225}{0.00015} = -10001.5
\end{aligned}$$

From these calculations we can see the third column of the projection matrix has incorrect sign, because the  $P_{3,2}^{formal}$  should be 1 and instead it is -1, and the far clip is negative, which should not be. When changing signs of third column of projection matrix, we obtain following formal definition of projection matrix. That sign switching means the view frustum is in opposite direction of Z axis.

$$P^{formal} = \begin{bmatrix} \frac{f}{r} & 0 & 0 & 0 \\ 0 & \frac{f}{t} & 0 & 0 \\ 0 & 0 & -\frac{n}{n-f} & -\frac{fn}{n-f} \\ 0 & 0 & -1 & 0 \end{bmatrix}$$

After fixing the sign issue, the relationship between  $P^{formal}$  and clips is

$$\begin{aligned}
\frac{P_{2,3}^{formal}}{P_{2,2}^{formal} + 1} &= n = \frac{1.500225}{0.00015 + 1} = 1.499999 \\
\frac{P_{2,3}^{formal}}{P_{2,2}^{formal}} &= f = \frac{1.500225}{0.00015} = 10001.5
\end{aligned}$$

As we can see, the  $n = 1.499999 \approx n_c = 1.5$  so for near clip, we can say we successfully reverse-engineered the relation between the projection matrix and the near clip. The far clip, on the other hand, differs  $f = 10001.5 \neq f_c = 800$ . The difference is very high, which lead us to assumption that there is some new far clip, which is not same as obtained through API,  $f_c$ .

The other check we can perform is projecting points laying on near clip and far clip into NDC space.

We prepare two points. Because of many zero elements in  $P^{formal}$ , we can see  $x$ -axis and  $y$ -axis don't affect the  $z$ -axis of projected point. Thus I prepared two points:

$$\begin{bmatrix} 1 & 1 \\ 1 & 1 \\ -1.5 & -800 \\ 1 & 1 \end{bmatrix}$$

, which are laying on the near clip and far clip, respectively. We would assume that they would be mapped to 1 and 0, respectively. The negative sign is here because in RAGE, the camera view frustum is in negative part of  $Z$  axis.

$$\begin{bmatrix} 1.210067 & 0 & 0 & -0.000004 \\ 0 & 2.144507 & 0 & 0.000002 \\ 0 & 0 & 0.00015 & 1.500225 \\ 0 & 0 & -1 & 0 \end{bmatrix} \begin{bmatrix} 1 & 1 \\ 1 & 1 \\ -0.15 & -800 \\ 1 & 1 \end{bmatrix} = \begin{bmatrix} 1.210063 & 1.210063 \\ 2.144509 & 2.144509 \\ 1.5 & 1.380225 \\ 1.5 & 800 \end{bmatrix}$$

by normalization we obtain

$$\begin{bmatrix} \frac{1.210063}{1.5} & \frac{1.210063}{800} \\ \frac{2.144509}{1.5} & \frac{2.144509}{800} \\ \frac{1.50045}{1.5} & \frac{1.620225}{800} \\ \frac{1.5}{1.5} & \frac{800}{800} \end{bmatrix} = \begin{bmatrix} 0.80670867 & 0.00151258 \\ 1.42967267 & 0.00268064 \\ 1 & 0.00172528 \\ 1 & 1 \end{bmatrix}$$

from which we can see the near clip  $n_c$  is being projected correctly, but far clip  $f_c$  is not being projected into 0 and that true far clip  $f$  is behind this far flip  $f_c$ . These calculations give us some insight into projection matrix and its role in far clip estimation, but for more robust estimate, I analysed all 33293 matrices. In GTA, matrices are not gathered correctly every time and in some cases, resulting matrices are unusable. Because I knew the near clip precisely, I discarded all matrices, with calculated near clip with difference from real near clip  $> 10^{-4}$ . For the rest of matrices, I calculated near clip and far clip for each of them. In the figure 5.3 can be seen histograms of these calculated far clip and near clip for each matrix, respectively. Even near clip values, which we know precisely, differ, but with very little variance, in range  $[1.5003, 1.50048]$  which means difference from true near clip in range  $[3 \cdot 10^{-4}, 4.8 \cdot 10^{-4}]$  which is simply explained by numerical instability. Both histograms have logarithmic  $y$  scale, so we easily see which value occurs more frequently. The value  $-10003.814$  occurred most frequently in matrices, one and half order of magnitude more frequently than second frequent value, and this value also corresponds to the median of all calculated far clips. Thus this far clip  $F = -10003.814$  has been used in all later experiments as a true far clip.

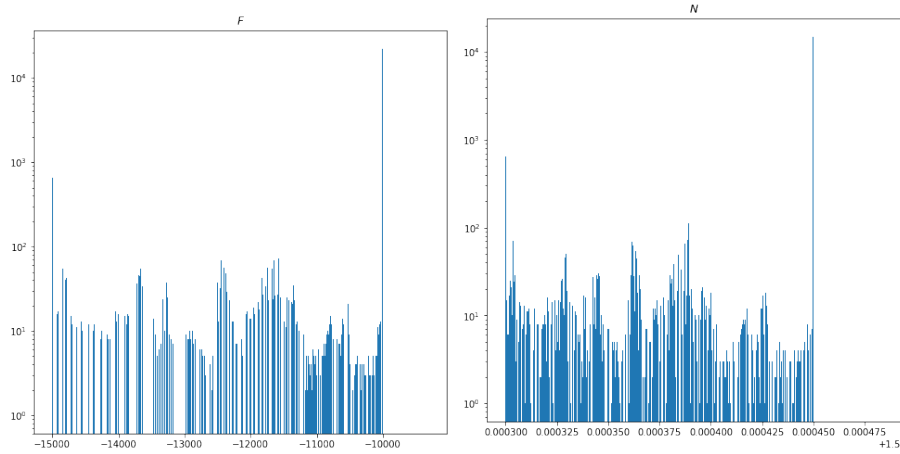
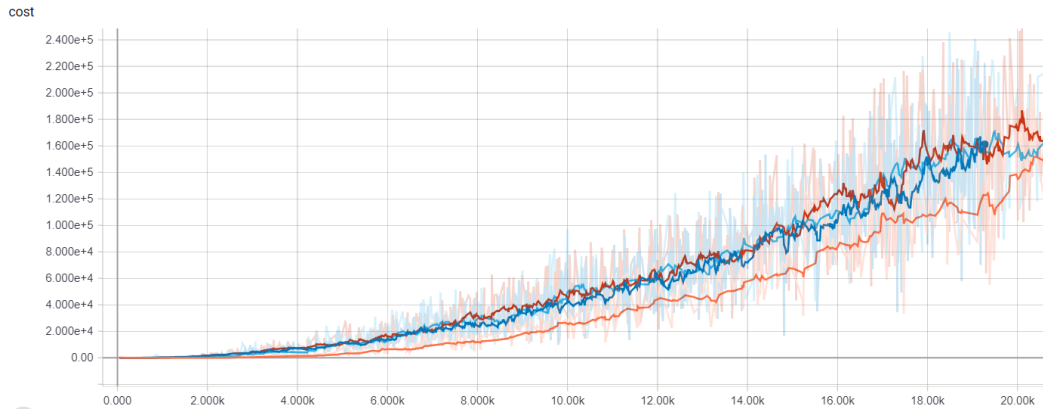
Figure 5.3.: Frequencies of  $P_{2,2}$  and  $P_{2,3}$ 

Figure 5.4.: Failing to learn

## 5.2. Depth estimation

For all experiments, the same network architecture has been used, only hyper-parameters were being tuned. The initial experiments started with 201 depth bins, as used in [41] but with additional depth bin for more distant depth values. But the network failed to learn in this setup. The cost increased exponentially instead of decreasing, as can be seen in figure 5.4. The cost function which was being minimized in this setup was the multinomial loss, as described in 2.1. With time, cost function was increasing. In the run denoted by light blue colour, only 40 training images were fed into the network, to try if it is able to remember patterns, without any requirement of generalization. As can be seen, even in this setup network failed to learn. All runs are runs with different learning rates, in expectation that lower learning rate would prevent this cost explosion, but it did not seem to have any effect at all. The training and validation data from dataset were split in 80/20 ratio.

After reducing the output number of depth levels to 101, 100 depth levels and one remaining level for all depth values outside the binned range, network started to learn, as. The training was then run in multiple setups, to find the best predictor. 9 setups will be discussed. Setups

name	optimizer	decay after	training time	iterations
setup 1	Adam(epsilon= $10^{-8}$ )	$2 \cdot 10^4$ steps	58h	237k
setup 2	Adam(epsilon= $10^{-8}$ )	$3 \cdot 10^4$ steps	26h	164k
setup 3	Nadam(epsilon= $10^{-8}$ )	$3 \cdot 10^4$ steps	26h	105k
setup 4	Adam(epsilon= $10^{-5}$ )	$3 \cdot 10^4$ steps	26h	175k
setup 5	Nadam(epsilon= $10^{-5}$ )	$3 \cdot 10^4$ steps	30h	202k
setup 6	Nadam(epsilon= $10^{-2}$ )	$3 \cdot 10^4$ steps	30h	189k
setup 7	Nadam(epsilon= $10^{-8}$ )	no decay	30h	120k
setup 8	SGDN(momentum=0.999)	no decay	26h	184k
setup 9	SGDN(momentum=0.9)	no decay	26h	108k

Table 5.1.: Depth estimation setups

parameters can be seen in the table 5.1. As a loss function, the information gain based loss in 2.2 has been used. The initial learning rate is same for all setups. The Nadam optimizer is abbreviation for Adam optimizer with Nesterov momentum. For all runs using Adam and Nadam optimizers, only epsilon parameter was tuned, beta1 and beta2 parameters were constant, beta1=0.9, beta2=0.999. The SGDN is abbreviation for the stochastic gradient descent with Nesterov momentum. The initial learning rate was set to  $10^{-4}$  for all runs. For setups 1 to 6, learning rate decay has been used. The learning rate decay is staircase, after a period given in “decay after” column the learning rate is divided by 10. For runs 7 to 9, learning rate remained unchanged for all training. Networks were trained on different GPUs, namely, Nvidia Titan Xp, Titan X, and Nvidia GTX 1080Ti. Due to different computation capability of these cards and different number of CUDA cores, run times are not highly correlated with number of iterations.

Metrics for depth estimation and loss have been calculated for the validation dataset on these 9 setups, they can be seen in table 5.2. The accuracy under threshold 1.25 (*aut* (1.25)) is in range  $[0, 1]$  by definition. 0 accuracy means depth in not pixel is in range from  $\frac{1}{1.25} = 0.5$  to 1.25 of ground truth depth, 1 accuracy means all pixels are in 0.8 to 1.25 of ground truth depth. All these calculations are done on reconstructed images, meaning higher accuracy means better models. Error metrics measure error rate and thus lower error means better model. Some metrics highly correlate with each other, showing they describe similar information. From accuracy under threshold and root mean squared log error (*rmls*) we can see setups 6,8,9 perform far worse than other models. So we can see generally SGDN performed worse than Adam and Nadam optimizers. From Adam and Nadam optimizers, the setup 7 performed the best, which is Nadam optimizer with epsilon= $10^{-8}$  and without the learning decay. That can be seen in all metrics except of mean relative error.

Few images from the validation dataset and their depth predictions can be seen in figure 5.5. In the first row, we can see the RGB image, in the second row is the ground truth depth in meters. The third row depicts ground truth images reconstructed by the soft-sum inference from depth level bins. Here we can see all information behind 50 meters in truncated, which also visually helps us to focus on near objects. The red colour is for nearer objects and blue colour is for more distant objects. In rows 4-7 we can see the predictions of setups 3, 4, 5 and 7 which are performing better than rest of setups.

In the figure 5.6 we can see the loss during training and in figure 5.7 we can see all metrics gathered during training. Interesting property of loss function based on information gain is the fact that it does not seem to converge most of the time during training, but all metrics are being

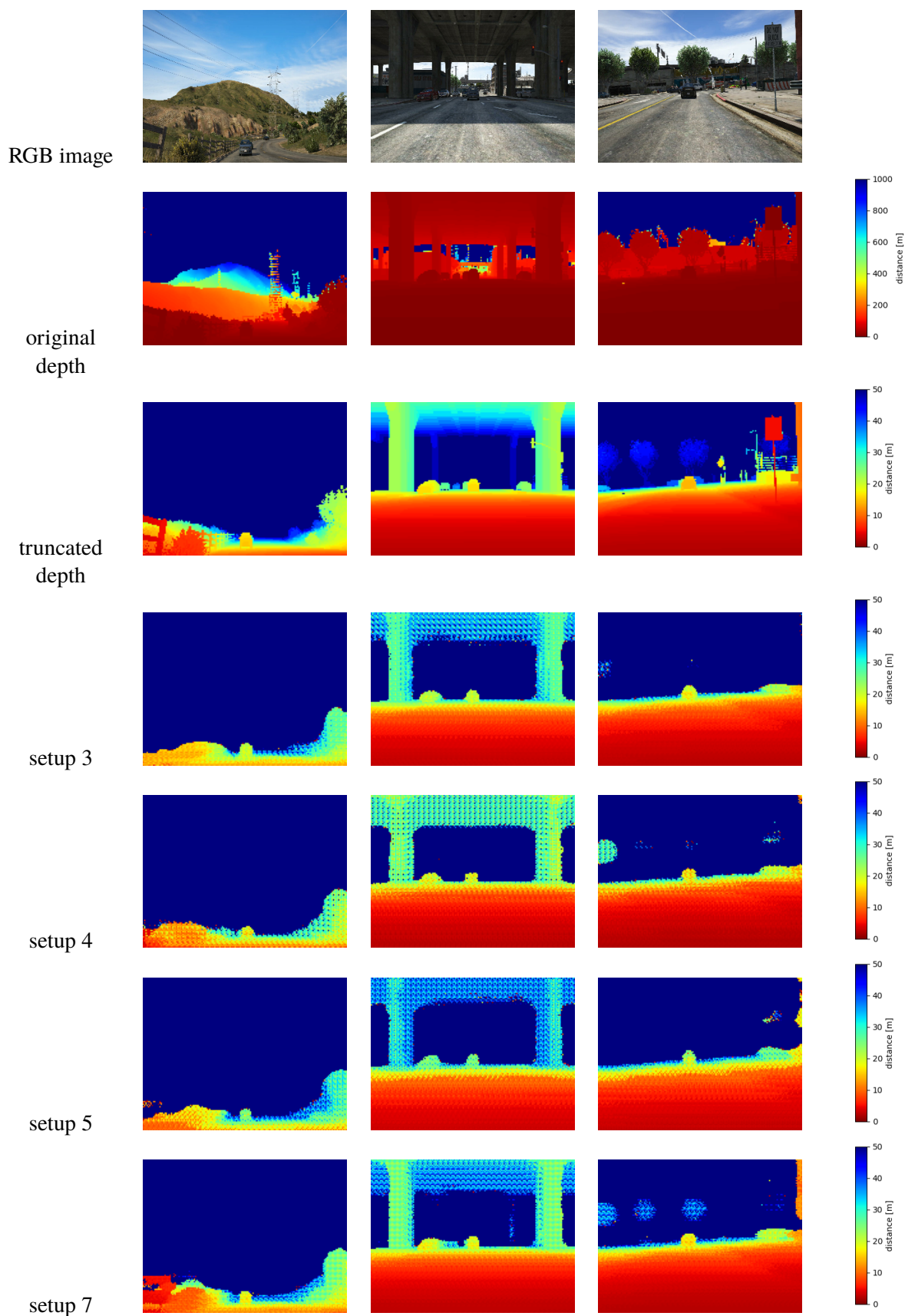


Figure 5.5.: Depth estimation samples



name	<i>aut</i> (1.25)	mean relative error	<i>rms</i>	<i>rmls</i>	average $\log_{10}$ error	loss
setup 1	0.4390	0.3607	10.7808	0.5415	0.2880	14.6054
setup 2	0.4393	0.3432	11.0467	0.5533	0.2926	14.5629
setup 3	0.4554	0.3287	10.3699	0.5219	0.2730	14.5234
setup 4	0.4258	0.3392	9.7831	0.4849	0.2620	14.5913
setup 5	0.4314	0.3394	10.2730	0.5066	0.2708	14.6061
setup 6	0.0390	0.6588	13.8523	0.8978	0.6960	14.8873
setup 7	0.4852	0.3494	8.2342	0.4140	0.2180	14.5132
setup 8	0.0	0.7106	13.9028	0.9403	0.7651	14.9104
setup 9	0.0508	0.6488	13.8551	0.8948	0.6873	14.8796

Table 5.2.: Depth estimation metrics



Figure 5.6.: Training for depth estimation - loss

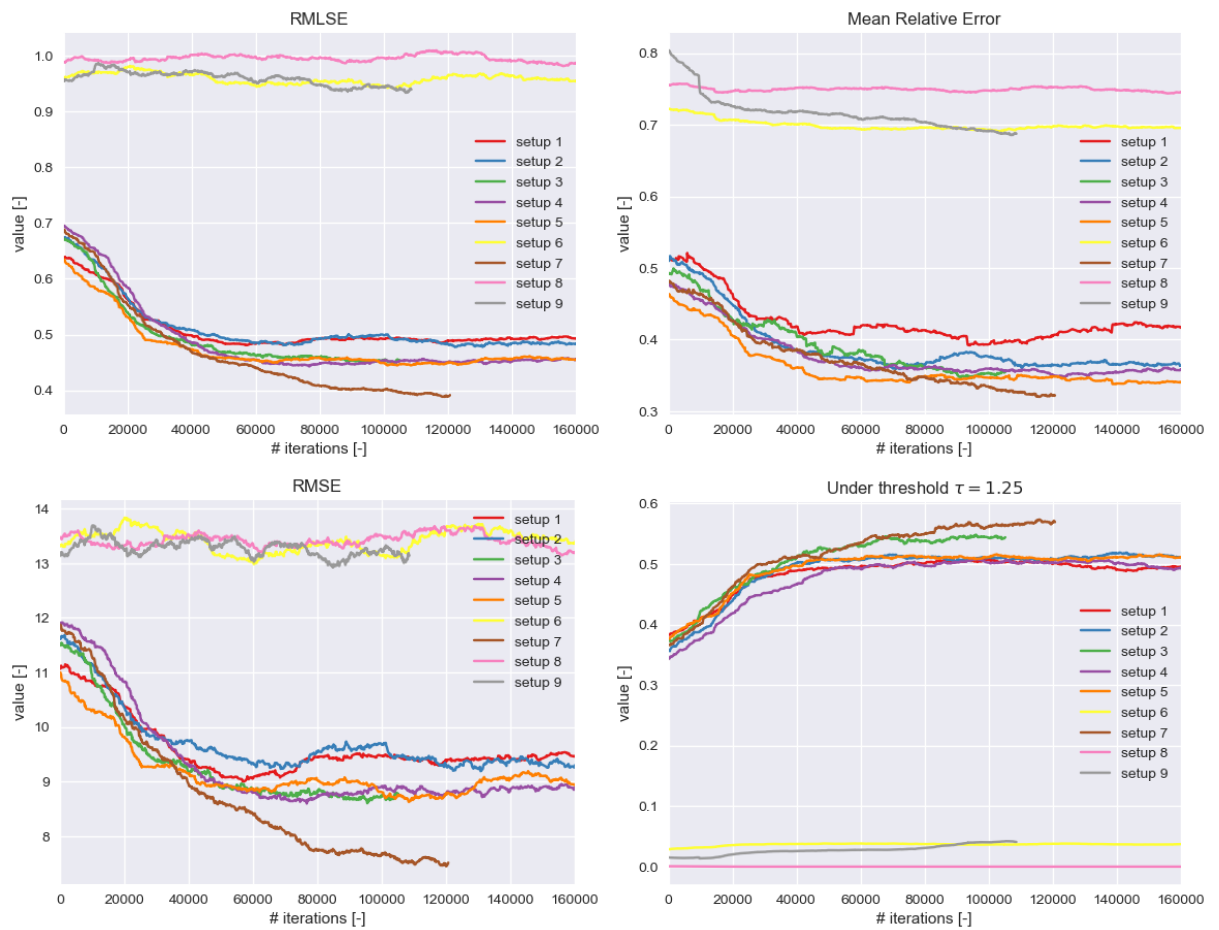


Figure 5.7.: Training for depth estimation - metrics

name	loss	optimizer	new deconvolutional layer	training time	iterations
setup 1	logistic	Nadam	-	25h	141k
setup 2	logistic	SGDN	-	24h	150k
setup 3	logistic	Nadam	kernel=5, stride=1,out_dim=50	28h	147k
setup 4	logistic	Nadam	kernel=2, stride=2,out_dim=50	44h	187k
setup 5	logistic	Nadam	kernel=2, stride=2,out_dim=200	52h	154k

Table 5.3.: 3D estimation setups

name	false positive rate	true positive rate	intersection over union	$l_1$ distance	loss
setup 1	0.2732	0.8603	0.6523	12151.0	0.1244
setup 2	0.0505	0.4712	0.2214	64437.4	0.13013582
setup 3	0.2120	0.8369	0.6233	13386.8	0.1080089
setup 4	0.2250	0.8355	0.6192	13587.4	0.097417
setup 5	0.2356	0.8514	0.6730	12359.5	0.123826

Table 5.4.: Depth estimation metrics

optimized even when it is not seen in the loss figure. Here we can see clearly how setups 6, 8 and 9 performed poorly and setup 7 performed the best in all metrics. The setup 7, which is Adam optimizer with Nesterov momentum, a.k.a. Nadam optimizer with constant learning rate seems to have best results and thus is used as a default optimizer for 3D map estimation and learning rate is constant in all setups.

### 5.3. 3D map estimation

For 3D map estimation, I also trained multiple setups and evaluated them, 7 of them with most promising results are discussed here. The architecture was being modified, the last softmax layer was removed because now we don't aim to predict occupation of only 1 depth voxel per pixel, but we can predict multiple occupied voxels. Also, for setups 5, 6 and 7, new deconvolutional layer was stacked, between the last convolutional layer and the deconvolutional layer before the output. The parameters for optimizer were same,  $\epsilon=10^{-8}$ ,  $\beta_1=0.9$ ,  $\beta_2=0.999$  for Nadam optimizer, and  $\text{momentum}=0.9$  was used for SGD optimizer with Nesterov momentum. For all setups, the weighted logistic loss 4.1 is used. We can see the overview in the figure 5.3. Then I evaluated these setups on validation sets and reported results in the table 5.4.

The process of training is shown in figures 5.8 and 5.9. In figure 5.8 we can see the cost being minimized. Here the logistic loss itself shows how individual setups perform. The figure has logarithmic Y scale for better visualization of individual setups. In the figure 5.9 we can see metrics. The false positive rate is very low for all runs, but for other metrics we can see stochastic gradient descent with Nesterov momentum (setup 2) performed much poorer than other run. On the other hand, the setup 1 and setup 5 perform better than other setups in all metrics. From this we can than reduction of 4th dimension to the size of 50 in the end of the network worsens the performance, on the other hand, adding layer with 4th dimension of size 400 performs better in intersection over union metric.

In figure 5.10 we can see two sample images from validation dataset, their ground truth

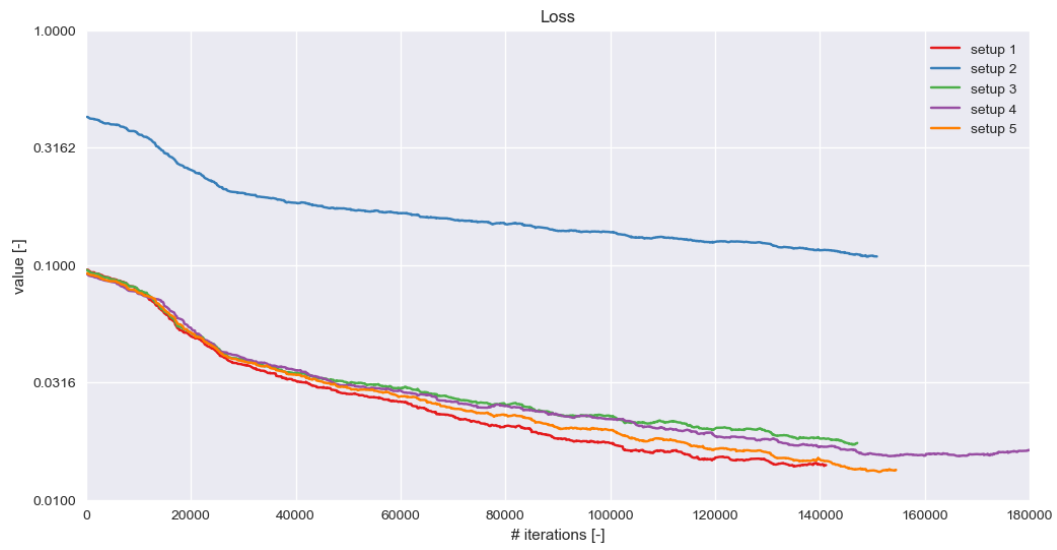


Figure 5.8.: Training for 3D map estimation - loss

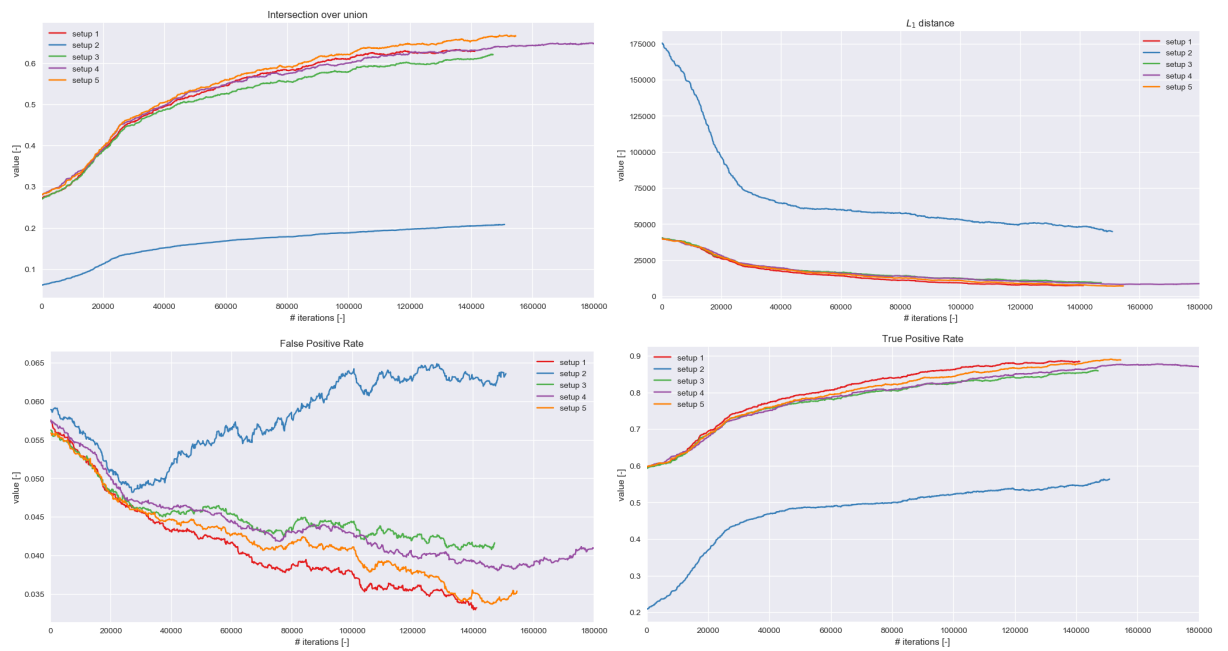


Figure 5.9.: Training for 3D map estimation - metrics

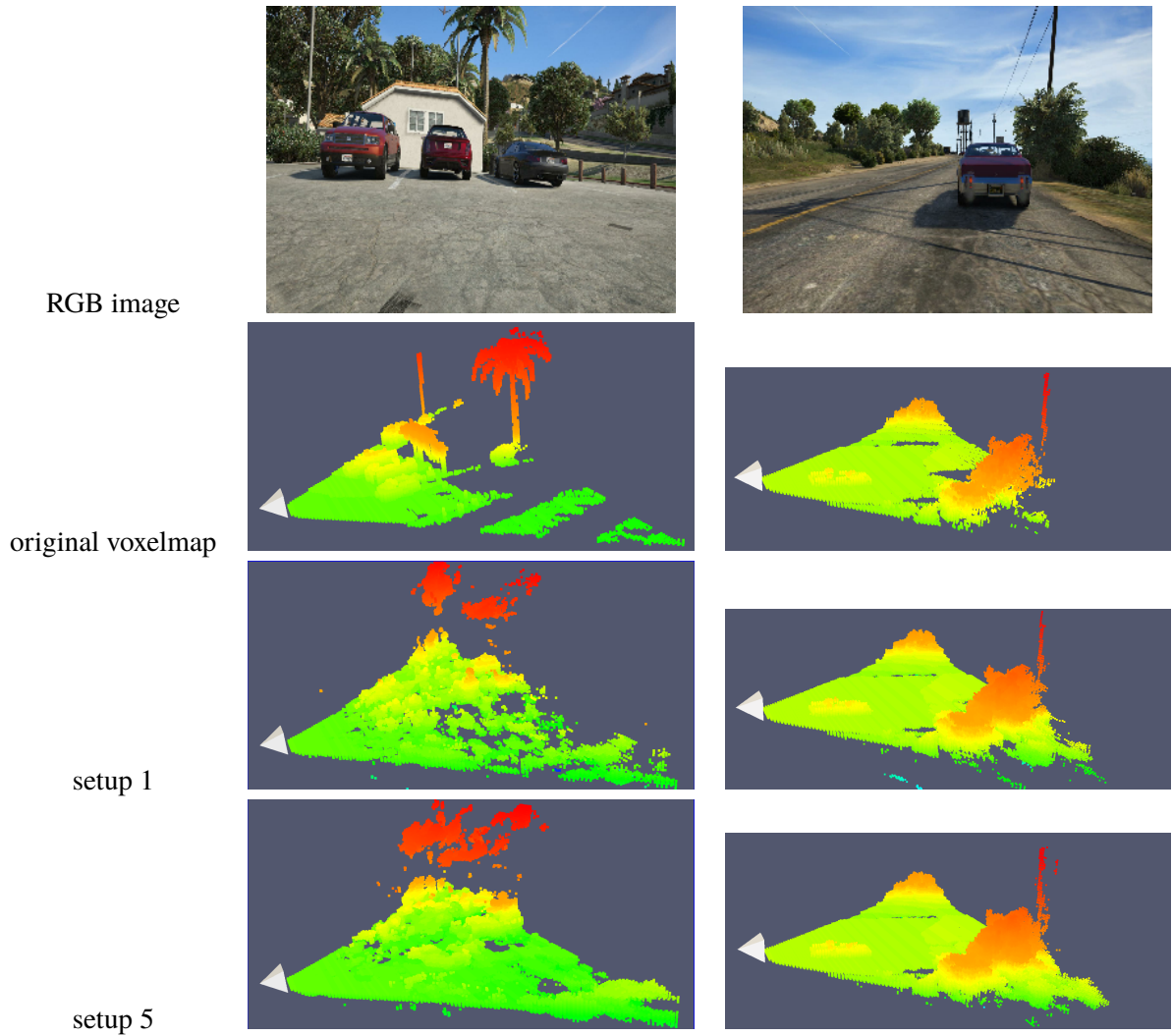


Figure 5.10.: 3D estimation samples

voxelmaps and predicted voxelmaps from 2 best setups, setup 1 and setup 5. In the first row, we can see the input image to the network, in the second row is the ground truth voxelmap in camera view frustum (and camera position denoted by white tetrahedron), and the last two rows show predictions of setup 1 and setup 5, respectively.

## CONCLUSION AND FUTURE WORK

This thesis contributed to the reactive depth and 3D estimation by proposing a deep neural network architecture for depth and 3D estimation from single RGB image. The trained neural network works well for roads-like images with fixed camera field of view. The number of depth bins showed to be essential for the ability of network to learn the depth estimation correctly. In conclusion, I proposed neural network architecture for both depth and 3D estimation and evaluated it with multiple hyper-parameters. I demonstrated an automatic synthetic dataset creation and labels gathering from rich virtual world of GTA V for dense labelling of data. Then I reverse-engineered camera parameters and parameters of RAGE visualization pipeline and described an API used to control the virtual world and manipulate it during data gathering. I proposed synthetic dataset gathered by aforementioned method and then used this dataset for training neural network for depth and 3D map estimation tasks. I compared multiple optimizers for depth estimation and evaluated their performance. Adam optimizer with Nesterov momentum shown to perform better than Adam optimizer, which is seen by many as a default optimizer for most of tasks, and it also shown to perform better than SGD optimizer with Nesterov momentum. Lastly, I trained neural network for 3D map estimation and evaluated several network architecture changes. Compressing the network capacity of the network in the end of the structure from 101 dimension size to the dimension size of 50 and back to 101 shown to worsen the accuracy, on the other hand increasing the dimension size to 200 between last convolution layer and last layer improved only union over intersection, but did not outperform model without additional layer in other metrics.

During working with GTA V, many aspects have been discovered, but even more of them remained to be discovered in the future. In GTA V reverse-engineering, many stencil values semantics remain to be interpreted. Also, in GTA V, the modding capabilities are far from using their full potential. Lots of existing mods could help with scenarios setup for gathering data in specific situations, also necessary tooling needs to be developed to provide simple interface for scenarios setup. But probably one of the most promising mod categories are visual mods, which enhance the graphics of the game. Many visual mods are being used currently and some of them can be combined together, utilizing advantages of them both. The main difficulty in using visual mods is evaluation of their photo-realism. In the gaming community, players long for stunning graphics and aesthetically pleasing visuals. These visuals are sometimes unfortunately different than photorealistic visuals. Even when surveying individual players for most realistic visual mod, most of them considered as realistic the most aesthetically pleasing mod, without considering

---

the photorealism to be relevant. Photorealism of individual visual mods and their combination should be exploited and evaluated in order to get even more photo-realistic visual data. There are multiple visual mods, namely Redux, Make Visual Great Again, Natural Vision Remastered, Rhancer Photorealism Mod, VisualV, K-putt's SweetFX Config (ReShade). The problem with evaluation of these mods is missing support of tooling for automated manipulation with GTA, mods need to be installed and uninstalled manually, same goes for starting the game which leads to slow and time-consuming evaluation of photorealism of these mods, but it definitely is worth it in the long term. Also developing custom visual mod which would make the game look more photorealistic would solve this problem. Also streets layout and static assets can be changed by mods and if changed correctly, they would better simulate real-life environment. Current setting of GTA V is heavily based on Los Angeles, so street layout, house architectures, cars and other objects are set to correspond with Los Angeles. This layout differs in other parts of world and many use-cases would profit from possibility of using more European or other streets layout, cars and houses architecture. Other notable aspect of the game is possibility to render multiple cameras at time, allowing to capture stereo data in real-time without switching between them or speeding up data gathering from multiple cameras. So far GTA V is VR ready which means it already supports stereo-camera rendering, and so it awaits for being used in data gathering. Other potentially perspective, but yet not unexplored usage of GTA V is multiplayer setup, which can be used for multi-agent simulations. The official multiplayer of course does not allow using any modifications, but there is FiveM, program for running private GTA V server on dedicated machines, with support for server-side and client-side scripting, which could be used for many multi-agent tasks.

The network has been trained only on synthetic data in single weather, in further work creating mixed dataset would help to generalize by greater diversity between individual samples. The network setup currently depends of camera field of view and so this is a limiting factor for usage of with various cameras. Generalization of the current approach to be less dependent on camera field of view would improve the robustness of the model. Further work might also focus on estimation in different weather conditions and lightning settings.

## BIBLIOGRAPHY

- [1] Amazon mechanical turk product details. URL <https://www.mturk.com/product-details>.
- [2] Gta5-mods.com - your source for the latest gta 5 car mods, scripts, tools and more., . URL <https://www.gta5-mods.com/>.
- [3] Gta5 mods forum, . URL <https://forums.gta5-mods.com/category/5/general-modding-discussion>.
- [4] Gta forums, . URL <http://gtaforums.com/forum/370-gta-v/>.
- [5] Vehicles - gta 5 wiki guide - ign, . URL <http://www.ign.com/wikis/gta-5/Vehicles>.
- [6] Supervise.ly. URL <https://supervise.ly/>.
- [7] Martín Abadi, Ashish Agarwal, Paul Barham, Eugene Brevdo, Zhifeng Chen, Craig Citro, Greg S. Corrado, Andy Davis, Jeffrey Dean, Matthieu Devin, Sanjay Ghemawat, Ian Goodfellow, Andrew Harp, Geoffrey Irving, Michael Isard, Yangqing Jia, Rafal Jozefowicz, Lukasz Kaiser, Manjunath Kudlur, Josh Levenberg, Dandelion Mané, Rajat Monga, Sherry Moore, Derek Murray, Chris Olah, Mike Schuster, Jonathon Shlens, Benoit Steiner, Ilya Sutskever, Kunal Talwar, Paul Tucker, Vincent Vanhoucke, Vijay Vasudevan, Fernanda Viégas, Oriol Vinyals, Pete Warden, Martin Wattenberg, Martin Wicke, Yuan Yu, and Xiaoqiang Zheng. TensorFlow: Large-scale machine learning on heterogeneous systems, 2015. URL <https://www.tensorflow.org/>. Software available from tensorflow.org.
- [8] Tomas Akenine-Möller, Eric Haines, and Naty Hoffman. *Real-Time Rendering 3rd Edition*. A. K. Peters, Ltd., Natick, MA, USA, 2008. ISBN 987-1-56881-424-7.
- [9] Christopher M. Bishop. *Neural Networks for Pattern Recognition*. Oxford University Press, Inc., New York, NY, USA, 1995. ISBN 0198538642.
- [10] Alexander Blade. Native db. URL <http://www.dev-c.com/nativedb/>.
- [11] Alexander Blade. Native db script/native documentation and research, June 2014. URL <http://gtaforums.com/topic/717612-v-scriptnative-documentation-and-research/>.



- [12] Alexander Blade. Script hook v, April 2015. URL <http://gtaforums.com/topic/788343-script-hook-v/>.
- [13] Greg Brockman, Vicki Cheung, Ludwig Pettersson, Jonas Schneider, John Schulman, Jie Tang, and Wojciech Zaremba. Openai gym. *CoRR*, abs/1606.01540, 2016. URL <http://arxiv.org/abs/1606.01540>.
- [14] Gabriel J. Brostow, Julien Fauqueur, and Roberto Cipolla. Semantic object classes in video: A high-definition ground truth database. *Pattern Recogn. Lett.*, 30(2):88–97, January 2009. ISSN 0167-8655. doi: 10.1016/j.patrec.2008.04.005. URL <http://dx.doi.org/10.1016/j.patrec.2008.04.005>.
- [15] Yuanzhouhan Cao, Zifeng Wu, and Chunhua Shen. Estimating depth from monocular images as classification using deep fully convolutional residual networks. *CoRR*, abs/1605.02305, 2016. URL <http://arxiv.org/abs/1605.02305>.
- [16] Christopher Bongsoo Choy, Danfei Xu, JunYoung Gwak, Kevin Chen, and Silvio Savarese. 3d-r2n2: A unified approach for single and multi-view 3d object reconstruction. *CoRR*, abs/1604.00449, 2016. URL <http://arxiv.org/abs/1604.00449>.
- [17] Marius Cordts, Mohamed Omran, Sebastian Ramos, Timo Rehfeld, Markus Enzweiler, Rodrigo Benenson, Uwe Franke, Stefan Roth, and Bernt Schiele. The cityscapes dataset for semantic urban scene understanding. *CoRR*, abs/1604.01685, 2016. URL <http://arxiv.org/abs/1604.01685>.
- [18] Crosire. Community script hook v .net, April 2015. URL <https://github.com/crosire/scripthookvdotnet>.
- [19] Kevin Crowston. Amazon mechanical turk: A research tool for organizations and information systems scholars. In Anol Bhattacharjee and Brian Fitzgerald, editors, *Shaping the Future of ICT Research. Methods and Approaches*, pages 210–221, Berlin, Heidelberg, 2012. Springer Berlin Heidelberg. ISBN 978-3-642-35142-6.
- [20] Cyron43. Vautodrive, July 2015. URL <https://www.gta5-mods.com/scripts/vautodrive>.
- [21] David Eigen and Rob Fergus. Predicting depth, surface normals and semantic labels with a common multi-scale convolutional architecture. *CoRR*, abs/1411.4734, 2014. URL <http://arxiv.org/abs/1411.4734>.
- [22] Artur Filipowicz. Driving school ii video games for autonomous driving. resreport, Princeton University, May 2016. URL <http://orfe.princeton.edu/~alaink/SmartDrivingCars/Visitors/FilipowiczVideoGamesforAutonomousDriving.pdf>.
- [23] MICHAEL FRENCH. Inside rockstar north - part 2: The studio, October 2013. URL <https://www.mcvuk.com/development/inside-rockstar-north-part-2-the-studio>.
- [24] Rockstar Games. Grand theft auto v is coming 9.17.2013, January 2013. URL <https://www.rockstargames.com/newswire/article/48591/grand-theft-auto-v-is-coming-9172013.html>.

- [25] Rockstar Games. Grand theft auto v release dates and exclusive content details for playstation 4, xbox one and pc, September 2014. URL <https://www.rockstargames.com/newswire/article/52308/grand-theft-auto-v-release-dates-and-exclusive-content>.
- [26] Andreas Geiger, Philip Lenz, Christoph Stiller, and Raquel Urtasun. Vision meets robotics: The kitti dataset. *International Journal of Robotics Research (IJRR)*, 2013.
- [27] Xavier Glorot and Yoshua Bengio. Understanding the difficulty of training deep feed-forward neural networks. In Yee Whye Teh and Mike Titterton, editors, *Proceedings of the Thirteenth International Conference on Artificial Intelligence and Statistics*, volume 9 of *Proceedings of Machine Learning Research*, pages 249–256, Chia Laguna Resort, Sardinia, Italy, 13–15 May 2010. PMLR. URL <http://proceedings.mlr.press/v9/glorot10a.html>.
- [28] Guad. Native ui, July 2015. URL <https://github.com/Guad/NativeUI>.
- [29] A. Halevy, P. Norvig, and F. Pereira. The unreasonable effectiveness of data. *IEEE Intelligent Systems*, 24(2):8–12, March 2009. ISSN 1541-1672. doi: 10.1109/MIS.2009.36.
- [30] Kaiming He, Xiangyu Zhang, Shaoqing Ren, and Jian Sun. Deep residual learning for image recognition. *CoRR*, abs/1512.03385, 2015. URL <http://arxiv.org/abs/1512.03385>.
- [31] Kaiming He, Georgia Gkioxari, Piotr Dollár, and Ross B. Girshick. Mask R-CNN. *CoRR*, abs/1703.06870, 2017. URL <http://arxiv.org/abs/1703.06870>.
- [32] Matt Hill. Grand theft auto v: meet dan houser, architect of a gaming phenomenon, September 2013. URL <https://www.theguardian.com/technology/2013/sep/07/grand-theft-auto-dan-houser>.
- [33] Kurt Hornik, Maxwell Stinchcombe, and Halbert White. Universal approximation of an unknown mapping and its derivatives using multilayer feedforward networks. *Neural Networks*, 3(5):551 – 560, 1990. ISSN 0893-6080. doi: [https://doi.org/10.1016/0893-6080\(90\)90005-6](https://doi.org/10.1016/0893-6080(90)90005-6). URL <http://www.sciencedirect.com/science/article/pii/0893608090900056>.
- [34] Sergey Ioffe and Christian Szegedy. Batch normalization: Accelerating deep network training by reducing internal covariate shift. *CoRR*, abs/1502.03167, 2015. URL <http://arxiv.org/abs/1502.03167>.
- [35] M. Johnson-Roberson, Charles Barto, Rounak Mehta, Sharath Nittur Sridhar, Karl Rosaen, and Ram Vasudevan. Driving in the matrix: Can virtual worlds replace human-generated annotations for real world tasks? In *IEEE International Conference on Robotics and Automation*, pages 1–8, 2017.
- [36] Baldur Karlsson. Renderdoc. URL <https://renderdoc.org/>.
- [37] Y. LeCun. A theoretical framework for back-propagation. In P. Mehra and B. Wah, editors, *Artificial Neural Networks: concepts and theory*, Los Alamitos, CA, 1992. IEEE Computer Society Press.

- [38] Yann LeCun, Leon Bottou, Genevieve B. Orr, and Klaus Robert Müller. *Efficient Back-Prop*, pages 9–50. Springer Berlin Heidelberg, Berlin, Heidelberg, 1998. ISBN 978-3-540-49430-0. doi: 10.1007/3-540-49430-8\_2. URL [https://doi.org/10.1007/3-540-49430-8\\_2](https://doi.org/10.1007/3-540-49430-8_2).
- [39] Yann LeCun, Yoshua Bengio, and Geoffrey E. Hinton. Deep learning. *Nature*, 521(7553): 436–444, 2015. doi: 10.1038/nature14539. URL <https://doi.org/10.1038/nature14539>.
- [40] Bo Li, Chunhua Shen, Yuchao Dai, A. van den Hengel, and Mingyi He. Depth and surface normal estimation from monocular images using regression on deep features and hierarchical crfs. In *2015 IEEE Conference on Computer Vision and Pattern Recognition (CVPR)*, pages 1119–1127, June 2015. doi: 10.1109/CVPR.2015.7298715.
- [41] Bo Li, Yuchao Dai, and Mingyi He. Monocular depth estimation with hierarchical fusion of dilated cnns and soft-weighted-sum inference. *CoRR*, abs/1708.02287, 2017. URL <http://arxiv.org/abs/1708.02287>.
- [42] Thomas Morgan. Face-off: Grand theft auto 5, September 2013. URL <https://www.eurogamer.net/articles/digitalfoundry-grand-theft-auto-5-face-off>.
- [43] OpenAI. Openai-universe, December 2016. URL <https://blog.openai.com/universe/>.
- [44] Shaoqing Ren, Kaiming He, Ross B. Girshick, and Jian Sun. Faster R-CNN: towards real-time object detection with region proposal networks. *CoRR*, abs/1506.01497, 2015. URL <http://arxiv.org/abs/1506.01497>.
- [45] Stephan R. Richter, Vibhav Vineet, Stefan Roth, and Vladlen Koltun. Playing for data: Ground truth from computer games. In Bastian Leibe, Jiri Matas, Nicu Sebe, and Max Welling, editors, *European Conference on Computer Vision (ECCV)*, volume 9906 of *LNCS*, pages 102–118. Springer International Publishing, 2016.
- [46] Olga Russakovsky, Jia Deng, Hao Su, Jonathan Krause, Sanjeev Satheesh, Sean Ma, Zhiheng Huang, Andrej Karpathy, Aditya Khosla, Michael S. Bernstein, Alexander C. Berg, and Fei-Fei Li. Imagenet large scale visual recognition challenge. *CoRR*, abs/1409.0575, 2014. URL <http://arxiv.org/abs/1409.0575>.
- [47] Ashutosh Saxena, Sung H. Chung, and Andrew Y. Ng. Learning depth from single monocular images. In *Proceedings of the 18th International Conference on Neural Information Processing Systems, NIPS’05*, pages 1161–1168, Cambridge, MA, USA, 2005. MIT Press. URL <http://dl.acm.org/citation.cfm?id=2976248.2976394>.
- [48] D. Scharstein, R. Szeliski, and R. Zabih. A taxonomy and evaluation of dense two-frame stereo correspondence algorithms. In *Proceedings IEEE Workshop on Stereo and Multi-Baseline Vision (SMBV 2001)*, pages 131–140, 2001. doi: 10.1109/SMBV.2001.988771.
- [49] Jamie Shotton, Andrew Fitzgibbon, Andrew Blake, Alex Kipman, Mark Finocchio, Bob Moore, and Toby Sharp. Real-time human pose recognition in parts from a single depth image. In *IEEE. IEEE*, June 2011.

- [50] Karen Simonyan and Andrew Zisserman. Very deep convolutional networks for large-scale image recognition. *CoRR*, abs/1409.1556, 2014. URL <http://arxiv.org/abs/1409.1556>.
- [51] A. Sorokin and D. Forsyth. Utility data annotation with amazon mechanical turk. In *2008 IEEE Computer Society Conference on Computer Vision and Pattern Recognition Workshops*, pages 1–8, June 2008. doi: 10.1109/CVPRW.2008.4562953.
- [52] Rupesh Kumar Srivastava, Klaus Greff, and Jürgen Schmidhuber. Highway networks. *CoRR*, abs/1505.00387, 2015. URL <http://arxiv.org/abs/1505.00387>.
- [53] Chen Sun, Abhinav Shrivastava, Saurabh Singh, and Abhinav Gupta. Revisiting unreasonable effectiveness of data in deep learning era. *CoRR*, abs/1707.02968, 2017. URL <http://arxiv.org/abs/1707.02968>.
- [54] Christian Szegedy, Wei Liu, Yangqing Jia, Pierre Sermanet, Scott E. Reed, Dragomir Anguelov, Dumitru Erhan, Vincent Vanhoucke, and Andrew Rabinovich. Going deeper with convolutions. *CoRR*, abs/1409.4842, 2014. URL <http://arxiv.org/abs/1409.4842>.
- [55] Balázs Tukora and Tibor Szalay. High performance computing on graphics processing units. *Pollack Periodica*, 3:27–34, 08 2008. URL [https://www.researchgate.net/publication/242065578\\_High\\_performance\\_computing\\_on\\_graphics\\_processing\\_units](https://www.researchgate.net/publication/242065578_High_performance_computing_on_graphics_processing_units).
- [56] V4D3R. Gta-mod-dev-tutorial, August 2016. URL <https://forums.gta5-mods.com/topic/1451/tutorial-grand-theft-auto-v-modding-a-few-things-you-should-know/2>.
- [57] wozzy. Cameras - documentation, May 2015. URL <http://gtaforums.com/topic/793247-cameras/>.
- [58] Jun Xie, Martin Kiefel, Ming-Ting Sun, and Andreas Geiger. Semantic instance annotation of street scenes by 3d to 2d label transfer. *CoRR*, abs/1511.03240, 2015. URL <http://arxiv.org/abs/1511.03240>.
- [59] Fisher Yu and Vladlen Koltun. Multi-scale context aggregation by dilated convolutions. *CoRR*, abs/1511.07122, 2015. URL <http://arxiv.org/abs/1511.07122>.
- [60] M. Zahangir Alom, T. M. Taha, C. Yakopcic, S. Westberg, M. Hasan, B. C Van Esesn, A. A. Awwal, and V. K. Asari. The history began from alexnet: A comprehensive survey on deep learning approaches. *ArXiv e-prints*, March 2018.
- [61] Karel Zimmermann, Tomas Petricek, Vojtech Salansky, and Tomáš Svoboda. Learning for active 3d mapping. *CoRR*, abs/1708.02074, 2017. URL <http://arxiv.org/abs/1708.02074>.

## CONTENTS OF THE ENCLOSED CD

GTAVisionExport	Source code of GTA V mod
GTAVisionExport_Server	Gathering and data managing tools
data_postprocessing	Utility scripts for processing
voxelmap-estimation	Neural networks source code and dumps
diploma_thesis.pdf	diploma thesis PDF
diploma_thesis.tex	diploma thesis source
diploma_thesis.lyx	diploma thesis source
diploma_thesis_img	images for diploma thesis

